Improving Synchrophasor Estimation at Off-Nominal Power System Conditions using Discrete Fourier Transformations

By

Salish Maharjan

A Thesis Presented to the

Masdar Institute of Science and Technology

in Partial Fulfillment of the Requirements for the Degree of

Master of Science

In

Electrical Power Engineering

Improving Synchrophasor Estimation at Off-Nominal Power System Conditions using Discrete Fourier Transformation

By Salish Maharjan

A Thesis Presented to the Masdar Institute of Science and Technology in Partial Fulfillment of the Requirements for the Degree of

Master of Science in Electrical Power Engineering

May 2015

AUTHOR'S DECLARATION

I understand that copyright in my thesis is transferred to Masdar Institute of Science and Technology.

Author _____

RESEARCH SUPERVISORY COMMITTEE MEMBERS

Dr. Jimmy C. H. Peng, Chair, _____

Masdar Institute of Science and Technology

Dr. Weidong M. Xiao, _____

Masdar Institute of Science and Technology

Dr. Vinod Khadkikar, _____

Masdar Institute of Science and Technology

Abstract

Phasor Measurement Units (PMU) provide time-synchronized measurements of magnitude, phase angle, frequency, and rate of change of frequency at higher reporting rate in comparison with the conventional remote terminal unit (RTU) used by SCADA. Discrete Fourier Transformation (DFT) used by PMUs, usually designed at system frequency for phasor computation. As a result, leakage effect increases at large off-nominal frequency of the grid, which degrades the estimation from DFT. In order to enhance the accuracy of DFT during wide frequency deviations, two types of method based on frequency information were proposed in this research. The first approach is known as variable sampling time (VST) and the second is sample value adjustment (SVA). For frequency information, two estimators such as Biased Jacobsen and recursive least square (RLS), were used in VST and SVA methods, respectively. The combination of frequency and phasor estimators constitute an enhanced version of DFT, suitable for PMUs.

The MATLAB model of the proposed PMU designs were tested with various types of input signals as specified in the IEEE C37.118.1-2011 standard. The compliance of the designs with the standard were evaluated for steady and dynamic state by help of indices such as Total vector error (TVE), frequency error (FE), and rate of change of frequency error (RFE). Both the design demonstrated TVEs less than 1% and 3% at steady and dynamic states, respectively. Furthermore, the second design using SVA performed better than VST in terms of TVE and reporting rate. Because of this, the second design was implemented in prototype PMU and the measurements from it were visualized and recorded by LabVIEW. The recorded measurements were validated by determining the TVE and were in compliance with the standard.

This research was supported by the Government of Abu Dhabi to help fulfill the vision of the late President Sheikh Zayed Bin Sultan Al Nahyan for sustainable development and empowerment of the UAE and humankind.

Acknowledgments

First of all, I would like to thank Government of Abu Dhabi for granting graduate scholarship at Masdar Institute of Science and Technology. This thesis is the outcome of my enthusiasm and utilization of this opportunity.

I would like to convey my gratitude and appreciation to my advisor, Dr. Jimmy C. H. Peng and co-advisor, Micheal Weidong Xiao for their guidance and valuable suggestions throughout my graduate research. I would like to thank research supervisory committee for their invaluable suggestions and comments for enhancing my works.

Dr. Jimmy provided the summer internship opportunity at Massachusetts Institute of Technology, at which I worked with Jorge Elizondo Martinez, PhD. student of Prof. James Kirtley. He helped me to develop an idea about smart monitoring system and their necessity in current power system. A Special thanks goes to Jorge for his strong support in hardware design and firmware development of the PMU. I don't hesitate to say that this research work wouldn't be completed without his assistance. I would also like thank Dr. Haris Muhammad Khalid for his productive guidance in my research.

Last but not the least, I would like to acknowledge my family for their emotional support in every step of my graduation. I would also like to acknowledge my friend Jim and Jamrus for encouragement and motivational tips at every steps of difficult situation.

Salish Maharjan,

Masdar City.

Contents

List of Tables

List of Figures

CHAPTER 1

Introduction

Reliable electric grid is vital for large power networks such as the Eastern Interconnections in North America and the newly established GCC interconnections. An outage within the power grid has more detrimental economic impact than actual physical damage. It was estimated that the total economic loss due to north-east blackout in North America, which lasted for 4 days in August 2003, was about 6 billion dollar [1, 2]. The tripping of the Eastlake power plant in Cleveland was the precursor of the cascading failure. Analysis of phase angle from the measurement revealed a slow divergence nearly an hour before the blackout started [3]. A real-time phase angle monitoring system, if had been in use at the time, would allow system operators to be more aware of impending problem [4]. As a result, power utilities realized the significance of phasor monitoring system.

Due to advancement in power electronics and the increased environmental concerns, renewable generators like solar and wind became popular energy sources among utilities and consumers. The increasing penetration of renewable energy introduces new challenges into the conventional power system in terms of stability limits, reserve margins and voltage regulations [5, 6]. To address new operational issues, power system operators are emphasizing on the wide area monitoring system to update the state of their grids in real-time. Thus, better management of congested network can be achieved with wide-area monitoring, protection and control (WAMPAC) infrastructure which utilize the advance sensing, communicating, computing and visualizing technologies [8].

Synchrophasor meter is also known as Phasor Measurement Units (PMU) and these terms will be used interchangeably through out the thesis. It is a measuring device that computes magnitude, phase angle, frequency, and rate of change of frequency (ROCOF) while time-tagging the measurement instant. All the PMUs in the electric network are synchronized to a common reference time, which is usually served by the Global Positioning System (GPS). Time synchronized measurements help to know the state of the complete grid at any instant of time, and allows comparisons between measurements. This is very important for power operators to predict the detrimental consequences that might incur.

Power system is highly non-linear because of complex electromagnetic and electro-mechanical oscillations which occurs due to faults and interaction between the generators [7]. The complexity increases with the expansion of grid and increased intermittent resources. Most system operators rely on Energy Management System (EMS) security software to monitor the power grid. EMS utilizes the network model and telemetry data from the Supervisory Control and Data Acquisition (SCADA) system for determining the voltage magnitude and angles in all buses by using a state estimator. However, the estimation time of state estimator is within several seconds and is not able to capture the faster dynamics of grid. In contrast, the real-time PMUs directly measures phase angles at higher rate which allows operators to monitor the system continuously and adjust the conservative limits set by the off-line data. Consequently, the increased confident level of the security margins assist in operating network closer to the real stability limits [9].

In literature, synchronized phasor measurements have been used in many commercial monitoring applications like line impedance computation [10], model validation [11], congestion management [12], and tracking electromechanical oscillations [13, 14]. However, actual deployment of PMU-based applications are limited to few countries. This is mainly due to the cost of equipment, supporting infrastructure, and the limited operational successful stories. To date, United States, China, Spain, Italy, Korea and Japan have been installing PMUs into their grids for enhancing their SCADA systems. Meanwhile, France used PMUs in their coordinated protection schemes by centralized comparison of the voltage angles.

In general, power utilities believe PMU technology could contribute to enhancing the existing power grids in terms of reliability, robustness and security. The limitation towards a smarter power system operation is the associated cost of supporting communication and data acquisition infrastructures.

1.1 Motivation

Synchrophasor applications for steady-state operations are well established. It is also evident as the PMU standard published in 2005 only covered the performance requirement at steady-state. It was only in 2011, synchrophasors were demanded to meet certain accuracy under dynamic conditions [20].

The dynamic phasor estimation is an emerging field and the standard is being revised every couple of years. The conventional DFT used for static phasor computation degrades under dynamic signals and off-nominal conditions. Even using different windowing functions such as hamming and hanning, DFT is not able to provide the results that comply with the current standard. The current PMU utilizes enhanced DFT for phasor computation, which has several limitation for enhancing the computation speed and accuracy. The main drawback are computing the correction factor for frequency deviations and phase offsets due to average filter due to dependency of such factor with signal frequency and involves time consuming operations like multiple sine functions [17]. The easy implementation of enhanced DFT is done with the help of lookup table for correction and phase offset factor. The disadvantage of lookup table is that, the poor resolution of correction factor. This fact is taken as the mainstream algorithm for the PMU development. In order to capture the faster dynamics of power system, the PMUs should involve computational efficient algorithms, which ultimately increase its reporting rate. Reporting rate is one of the factor which distinguish PMUs from conventional RTUs.

The use of PMUs in wide-area monitoring system increases the situational awareness of the power network. It is very important to have an accurate monitoring system for both large interconnected power systems or a micro-grids. In any scenario, PMU measurements help to understand the interaction of the generators and load in real time. Another motivation of this thesis is to evaluate the fundamental working principles and challenges since many developed countries have started to understand the benefits of it.

Finally, the Abu Dhabi vision 2030 also incorporates deployment of demand side management in which the prosumers will be actively balancing the power grid along with the generators. To realize this vision, smart metering devices and communications will form the backbone of it. In order to integrate the PMU functions into smart metering device, the production cost should be minimized. The algorithms developed for this research was validated in protoype PMU, which could contribute in realizing the next generation smart meters.

1.2 Thesis Statement Objectives

Phasor estimation of the power grid during steady-state is more studied and such devices are commercially available. However, they fail to give the correct phasors during the dynamic condition. Power grid monitoring or protection is more significant in dynamic condition rather than steady-state. As a result, IEEE revised the standard recently and extended the performance index of the dynamic phasor estimators. Based on this new standard, the following are the main objectives of the research work:

- Design a phasor measurement unit for improving the phasor estimation at both steady and dynamic conditions.
- Test the proposed algorithms with input signals outlined in IEEE C37.118.1-2011 and evaluate the compliance.
- Validate the algorithms in a prototype of PMU.

1.3 Research Contributions

DFT is the commonly used technique by PMUs for phasor computation.Online implementation of DFT is not straight forward in power system because the frequency of grid is non-stationary. Frequency deviation from nominal value introduce higher TVE, which should be less than 1% even upto $\pm 5Hz$ as per the standard. The higher TVE at off-nominal frequency is due to leakage effect or due to signal discontinuity at edges of window. Although several window functions such as hamming window and hanning window can reduce the leakage effect for small frequency deviations, they are not effective under large frequency deviation. Current PMUs implement enhanced DFT, which requires a frequency information for computing the correction factor and phase offset factors. In this research, techniques of improving the accuracy DFTs were developed by the window tuning principle, which performed better than enhanced DFT in terms of accuracy and convergence speed. The constrains for DFT application in PMUs is time synchronization capability, which was taken into consideration as well.

Two types of real-time window tuning method based on frequency information were proposed in this research. The first approach utilize variable sampling time (VST) approach for tuning the window. The frequency information of input signal was estimated by using Jacobsen estimator for real-time implementation. This method is computationally efficient as it

do not need to recalculate the sample values or over-sample, but needs an extra time clock for synchronization with the GPS. The another limitation of it is that the maximum reporting rate is equal to the system frequency. Thus such algorithm is more suitable for developing Monitoring class PMU.

The second approach utilize sample value adjustment (SVA) technique for recalculating the samples to transform the signal off-nominal to nominal frequency. The frequency information for SVA was provided by recursive least square (RLS) estimator. The advantage of SVA is that with mild computation burden, you can get highly accurate phasor at higher reporting rate. The maximum reporting rate that can be achieved is equal to sampling frequency. Thus such algorithm is suitable for specially protection class PMU but can be also used for Monitoring class PMU.

Proposed PMU designs were complied with IEEE C37.118.1-2011 for both steady-state and dynamic state. Simulation and experimental results of both estimators demonstrated TVEs less than 1% and 3% at steady and dynamic states, respectively. Hence, the proposed designs could be used for single phase PMUs or can be integrated with smart meters, for distribution system.

1.4 Thesis Organization

The thesis is presented in the following layout:

Chapter1 begins with the several facts that urge the development of PMUs in the field of power system and then list out general application of it. The motivations, objectives and research contribution of the research are highlighted.

Chapter 2 describes the history and general structure of PMUs. Furthermore, the section also summarize the current approaches of phasor estimation for both steady and dynamic state of grid followed by the summary of the current IEEE standard C37.118.1-2011.

Chapter 3 presents the detail description of the DFT and theoretical modification of DFT for synchrophasor application. The proposed systems description and formulations are illustrated in the same chapter. In the end, the benchmark phasor estimating algorithm is described and compared with the proposed algorithms.

Chapter 4 illustrates the simulation and experimental results. Moreover, experimental setup and result validation are presented.

Chapter 5, finally concludes the research findings and outline future improvements required.

CHAPTER 2

Literature Review

2.1 Historical Overview

Phase angles contain critical information for determining the stability margins of power systems. In the past, measuring the angle difference between the two nodes of the transmission line was difficult because the time synchronization, computation and communication technologies were not matured. In 1980s, LORAN-C signal was used for synchronizing the clock of two measuring devices that were located 800 Km apart, and the phase angle was estimated by measuring the time to reach next zero-crossing from the reference time [15]. They were able to estimate the phase angle with maximum error of 1 degree. Similarly, the HBG radio was used for time synchronization in 1981 [16]. In both of these work, it is mentioned that the main source of error is due to error in time synchronization and demanding computational burden.

The enhancement in microprocessor technology and development of efficient algorithm for computing the symmetrical components in 1977 assisted in faster computation of the phasors. The Global Positioning System (GPS) was not completely deployed around 1980s. However, it offered an effective way of time synchronization over large distances. In the same year, the prototypes of PMU was developed in Virginia Tech and was later deployed in the substation of Bonneville Power Administration, American Electric Power Service Corporation and New York Power Authority [17]. By 1991, the GPS was in full-fledged and the first commercial PMU was introduced by Macrodyne in collaboration with Virginia Tech [18].

The first IEEE standard for synchrophasor was published in 1991 and was revised in 2005 [19]. Both of the standards focused only on the steady state requirement of synchrophasor. It was only in 2011 when the first draft of the dynamic synchrophasor requirement was released by IEEE [20]. At present PMUs are commercially available from different vendors and has been deployed in many countries for enhancing the conventional monitoring, protection and planning tools.

2.2 Overview of Phasor Measurement Unit

Phasor Measurement Units provides the synchronized phasors of voltage and current signals. Fig. 2.1 depicts on general block diagram of PMU. In the input stage, the power signals are filtered by a low pass filter to reject the high frequency noise and then the voltage and current transducers serve as a signal conditioner for interfacing with the digital system. The sampling frequency for the analog to digital converter (ADC) should be chosen according to Nyquist criteria in order to retain the characteristic of signal in discrete form [37]. It also determine the cut-off frequency of the low pass or anti-aliasing filter. The cut-off frequency is usually chosen less than half of the sampling frequency.

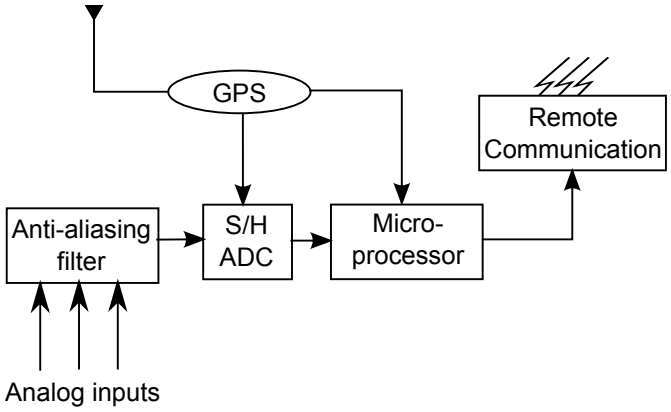

Figure 2.1: General block diagram of PMU

GPS is a reliable source of time synchronization in the deployment of PMU. Time synchronizing function in PMU is mainly for time tagging the measurements, which could be implemented in two ways.

1. By synchronizing the sampling frequency to a GPS clock, every sampling instant can be time tagged as the linear function sample index with reference to 1 PPS clock.

2. If sampling frequency is not constant, then in such case the current sample is time tagged

by summing the sampling time taken for each previous sample with reference to 1 PPS clock.

The first technique of time tagging is more widely used due to simplicity in implementation. Moreover, it has lower computational burden due to uniform sampling. The second time tagging technique is not commonly used in PMUs due to difficulty in summing the sampling time, which also top up computational burden. Such technique is only used when variable sampling frequency is employed, which is not very common in this field. Sampling rate in PMU is rising due to development of faster ADC and high end microprocessors and higher sampling rate also increases the accuracy and resolution of PMU [21]. In 1980s, the sampling rate of 12 samples per cycle was used in the first PMU developed by Virginia Tech where as the modern devices use 96 to 128 samples per cycle.

The phasor is computed for fundamental component in single phase system where as for three phase system, the positive sequence component is utilized to determine the phasor. Additionally, PMU also measures signal frequency and rate of change of frequency (ROCOF). Each measurement set is time tagged using universal coordinated time (UTC). Finally, the timed stamped measurement is communicated to the central server.

2.3 Nominal and Off-nominal Steady-State Phasor Estimation

Power grid is non-stationary system because of the continuous changes from load and generating station. However, the power system under nominal condition can be in quasi-steady state. In such case, the frequency, magnitude and phase angle of the power signal is almost constant or slowly drifting [19]. Phasor calculation for steady-state is well established and standardized in 2005. The steady-state could be at nominal frequency or at off-nominal frequency. At both cases, the phasor estimator should provide measurement with less than 1% total vector error [19].

Discrete Fourier Transform (DFT) is the commonly used technique for phasor calculations. DFT is the digital method of getting Fourier Transform [22]. The performance of DFT depends on the window length and the type of windowing function. Since, the frequency deviation in power system at steady-state is usually less than ± 2 Hz, the DFT is designed with the window length tuned for nominal frequency. The error is not significant for small frequency deviation but fails in large frequency deviation. One way of error minimization is using large window

length spanning over multiple cycles [17]. Another simple method of minimizing the error is by using window function such as Hanning or Hamming windows. The main source of error at off-nominal frequency is due to signal discontinuity at the edges of window, which is severe when rectangular window is employed. The Hanning or Hamming window uses a small weighting factor for the sample at edges while maintaining the highest weighting factor for the samples at center of the window. This reduces the signal discontinuity at edges of window and reduces the leakage phenomenon [23, 24]. But the demerit is that estimation delay grows with multiple cycle window length. So, in general 2 or 3 cycle window length is used for steady-state phasor estimation where as for dynamic phasor mostly 1 cycle window length is recommended [25]. It is proved in [25], the accuracy of hanning window DFT is higher than rectangular window DFT. Unfortunately, both methods fails to reduce TVE less than 1% for frequency deviation of $\pm$5 Hz. The frequency based compensation technique was used in [17] for correcting the DFT result. The correction factor were frequency dependent due to which the frequency estimator has also to be included. This technique along with instantaneous frequency estimation can also be used for dynamic phasor estimation.

2.4 Dynamic Phasor Estimation

The power signal is characterized by amplitude, frequency and phase angle. If any of them is varying with respect to time, it is regarded as dynamic or transient state. The transient state in power system can be categorized into two groups: a) electromagnetic transient and b) electromechanical transients [26].

2.4.1 Electromagnetic Transients

The electromagnetic transients are the result of switching and faults which produces the sudden change in voltage and current waveforms. Such transients add high frequency components in the signal for short period of time. Although , the anti-aliasing filter attenuates high frequency components, but the distortion of some magnitude propagates to ADC of the PMU. The distortion causes sudden change in the samples values affecting the data window of DFT. The phasor estimation with such data window is not valid which should be flagged properly for filtering out. One of such technique called transient monitoring scheme was illustrated in [17]. This research does not cover such monitoring mechanism to identify the invalid phasor.

2.4.2 Electromechanical Transients

Electromechanical transient are low frequency amplitude and phase angle modulations, caused due to interaction of the generators of power system, which are classified as inter-area oscillation or local oscillation [7]. Such oscillation typically range from 0.1 to 10 Hz. In some cases ramp variation of frequency was also observed [27]. Dynamic phasor should accurately estimate the phasor under all electromechanical transients and the accuracy level is defined in [20]. Frequency compensated DFT is one the technique for Dynamic Phasor Estimation. The main different between this algorithm when used only for steady-state estimation and for dynamic phasor estimation is the rate of frequency computation. Therefore, the dynamic phasor estimation is accompanied by instantaneous frequency which will be illustrated in the consequent sections.

2.5 Review of Existing Techniques for Dynamic Phasor Estimation

2.5.1 Frequency Compensation with DFT

The frequency compensated method described in [17] utilizes the compensating coefficient which are calculated based on the frequency deviation. The method suffers from a second harmonic oscillation in both magnitude and phase angle measurement for single phase case where as in three phase this effect is not observed. The demerit of this method is that the coefficient is complex in calculation and has a total vector error more than 1% at off-nominal conditions. The average filter was used in [28] for removing such oscillation in measurement. When the average filters are employed they also contribute in phase shift which is frequency dependent as well. Thus re-compensating the phase shift due to average filter, the method was able to reduce the TVE by less tha 1% at extreme off-nominal condition. The disadvantage of this method is that average filter phase shift is frequency dependent, which has to be calculated for each phasor estimation.

2.5.2 Window Tuning of DFT

The frequency-based window tuning is another method for phasor and frequency estimation. The benefits of this method is that it has relatively lower complexity in calculation. The window length is usually taken for one cycle of the signal for the sake of calculation speed. The window

length of the DFT is defined as $N * \Delta T$, where N and ΔT are samples per cycle and sampling time respectively. The window can be tuned by various methods which are described as follows.

Method 1: Window Tuning with Samples per Cycle

This is the simplest method of tuning the window length and the main objective is to make the window length exactly equal to the time period of the signal. This technique is employed for constant sampling frequency where the window length is tuned by adjusting N as per the frequency of input signal. The disadvantage of the method is that N can change only in discrete values where as the change in time period of signal is continuous. This method is not applicable for small frequency deviations and the tuning resolution is very poor. It is reported in [29] that the DFT with $N = 32$ cannot adjust N by unity unless there is frequency deviation of at least 1.935 Hz. Hence, this method is not suitable for dynamic phasor estimation.

Method 2: Window Tuning with Sampling time

Accurate DFT computation is be achieved by using this approach. This technique of computing DFT is employed in [30] for frequency measurement while developing a Volt/Hertz relay. The advantage is that, it does not need calculation of correction factors or re-sampling or sample value adjustment at off-nominal system frequency, which reduces the computational burden. The harmonic rejection for such DFTs is very effective until and unless sampling frequency is always an integer multiple of the system frequency [30]. However, for time synchronized measurement, this method is not easy to implement. It is advocated in [17] that for time tagging of the measurement with this method, the summation of sampling time of all previous sampling instant has to be calculated with reference to the GPS clock.

Method 3: Window technique with Interpolation

This is a sliding window with a constant N and sampling time approach and popular among the three window tuning techniques specially in PMU applications. Different strategies of interpolation could be used to operate it under off-nominal frequency. The Re-sampling technique was implemented in [31, 32] for accurate computation of synchronized phasors. It samples at higher rate and then re-sample to required rate which is multiple of the actual system frequency. The drawback of such over-sampling is the requirement of faster Analog to Digital converter and re-sampling adds computational burden on processor.

The sample value adjustment was used in [33, 28] which utilizes interpolation technique for converting the signal of off-nominal frequency to nominal frequency. The first order and second order spline approximation was used in former and later reference. The technique do not require over-sampling but need fair amount computation. The improvement on phasor estimation with this technique is significant at off-nominal frequencies as mentioned in [28] but dynamic capability was skipped. It did not assess the effect on accuracy with frequency estimator. Instead it assumed that the frequency is known by default which is not a realistic assumption for PMUs.

2.5.3 Phase Lock Loops

The conventional phase lock loops is well established for three-phase power system. It has a phase detector, loop filter and voltage control oscillator (VCO). The VCO tracks the frequency of the input signal and the integral gives the phase. The conventional phase lock loops suffers from double frequency ripples when the system is unbalanced and cannot be used for single phase case. The enhanced PLL was introduced in [34], which have many advantage over the conventional PLL. The first advantage is it can be used for single phase system and the second advantage is that it does not show second harmonic ripple even though the three phase system is unbalanced. The PLL loop in [34] was designed based on gradient descent method and was able to estimate phasors and frequency for both single and three phase system, which were in compliance with the C37.118.1-2011 standard.

2.5.4 Other Advance Methods

Alternative techniques other than DFT and PLL for phasor computation also exist in the literature such as using Fourier Tranform with phasor Taylor series [35] and wavelet based phasor estimator [36]. These techniques require high computational complexity and are difficult to implement in real time. Hence, they are not as popular as DFT based algorithm for commercial PMUs.

2.6 Summary of Synchrophasor Standard

The first synchrophasor standard, IEEE Std 1344 was published in 1995 and its successor IEEE Std C37.118 was released in 2005. These standard specified the performance of synchrophasor

only under the steady-state conditions. As monitoring and control of power system is more significant during transient case than steady state, the power engineers felt necessary to develop dynamic phasor estimators too. Many literature for steady-state phasor estimator forwarded the recommendations for dynamic phasor estimations. The accumulations of research and commercial experience in the field of synchrophasor, finally released a new standard in 2011, which incorporated the performance index for both dynamic and stead-state conditions. The minimum reporting rate for dyanmic phasors along with the test signals were also specified in the new standard. The standard also classified P and M class PMUs on the basis of accuracy level. This thesis proposes the PMU designs that are tested and verified as per the IEEE C37.118.1-2011 standard. The following subsection illustrates the measurement evaluation index and performance demanded by the new standard.

2.6.1 Measurement Evaluation

A. Total Vector Error

The total vector error (TVE) considers both amplitude and phase error together. The TVE is computed in [20] as:

$$TVE(n) = \sqrt{\frac{(\hat{X}_r(n) - X_r(n))^2 + (\hat{X}_i(n) - X_i(n))^2}{(X_r(n))^2 + (X_i(n))^2}} \tag{2.1}$$

where,

$\hat{X}_r(n) =$ estimated real part of phasor

$\hat{X}_i(n) =$ estimated imaginary part of phasor

$X_r(n) =$ Actual real part of phasor

$X_i(n) =$ Actual imaginary part of phasor

B. Frequency Error and Rate of Change of Frequency Error

Frequency error (FE) and Rate of Change of Frequency error (RFE) are evaluated as:

$$FE = |f_{true} - f_{measured}|$$

$$RFE = |(df/dt)_{true} - (df/dt)_{measured}|$$

2.6.2 Steady-state Compliance

The compliance for PMU with reporting rate higher than 20 Hz is only highlighted in this section. The Table 2.1 and 2.2 list the performance index required for PMUs at steady-state operation. Additional details can be referred to IEEE C37.118.1-2011 [20].

Table 2.1: Steady-state Synchrophasor Measurement Requirements

Influence Quantity	Reference Condition	P class		M class	
		Range	Max TVE (%)	Range	Max TVE (%)
signal frequency $f_o + f_{dev}$	f_o	±2 Hz	1	±5 Hz	1
Phase angle with $f_{dev} < 0.25$	constant or slowly varying angle	$\pm\pi$ radians	1	$\pm\pi$ radians	1
Harmonic distortion	less than 0.2% (THD)	1% each harmonic up to 50^{th}	1	10% each harmonic up to 50^{th}	1

Table 2.2: Steady-state Synchrophasor Frequency and ROCOF Measurement Requirement

Influence Quantity	Reference Condition	P class			M class		
		Range	Max FE	Max RFE	Range	Max FE	Max RFE
Signal frequency	f_o	f_o±2	0.005 Hz	0.01	f_o±5 Hz	0.005 Hz	0.01
Harmonic distortion	less than 0.2% (THD)	1% each harmonic up to 50^{th}	0.005 Hz	0.01	10% each harmonic up to 50^{th}	0.025 Hz	6

2.6.3 Dynamic Compliance

The dynamic compliance specifies the performance index at step change, ramp change of the input signal as well as for modulated input signal. This section will also point out the dynamic performance for the PMUs with reporting rate higher than 20 Hz. For entire details, it is advised to follow C37.118.1-2011 [20].

Table 2.3: Synchrophasor Measurement using Modulated Test Signals

Modulation Level	Reference Condition	P class		M class	
		Range	Max TVE (%)	Range	Max TVE (%)
k_x=0.1, k_a=0.1	rated signal magnitude at f_o	modulation frequency 2 Hz	3	modulation frequency 5 Hz	3

k_x and k_a are amplitude and angle modulation factor

Table 2.4: Frequency and ROCOF Performance Requirements under Modulation Tests

Modulation Level	P class		M class	
	Max FE	Max RFE	Max FE	Max RFE
reference to modulation level and range specified in Tab. 2.3	0.06 Hz	3	0.3 Hz	30 Hz

Table 2.5: Synchrophasor Performance Requirements under Frequency Ramp Tests

Test signal	Reference Condition	Ramp rate	Class	Ramp rate	Max TVE
linear frequency ramp	rates signal & f_o at start	$\pm$ 1 Hz/s	P class	$\pm$ 2 Hz	1%
			M class	$\pm$ 5 Hz	1%

Table 2.6: Frequency and ROCOF Performance Requirements under Frequency Ramp Tests

Signal specification	Reference condition	Transition time	P class		M class	
			Max FE	Max RFE	Max FE	Max RFE
Ramp tests same as in Tab. 2.5	0 radian base angle	$\pm 2/F_s$ for start and end of ramp	0.01 Hz	0.1 Hz/s	0.005 Hz	0.1 Hz/s

CHAPTER 3

Proposed PMU Enhancement

3.1 Discrete Fourier Transformation

Fourier Transform decomposes any time domain signal x(t) into the frequency domain X(f), which possess the information of both magnitude and phase angle. However, for digital computation, Fourier Transform is not suitable because infinite samples of x(t) has to be considered [22]. Discrete Fourier Transform (DFT) provides the solution for calculating the Fourier transform from a small number of samples taken from an input signal x(t). For DFT of any signal, it has to be sampled at a regular interval, such that the sampling frequency is integer multiple of the signal frequency of x(t) and also satisfying the nyquist criterion of sampling. This ensures the absence of aliasing and no information is lost by sampling [37]. In real-time application, where the largest frequency component of signal is unknown, the input signal is band-limited by using low pass filter or anti-aliasing filters.

Consider the sampled signal that fall under the rectangular window function w(t), which is represented by y(t) in the equation below.

$$
\begin{aligned}
y(t) &= x(t)\delta(t)w(t) \\
or, y(t) &= \sum_{n=0}^{N-1} x(n\Delta T)\delta(t - n\Delta T)
\end{aligned}
\tag{3.1}
$$

The variable N represents the number of uniform spaced (ΔT) samples in the window length.

This sampled signal has a continuous Fourier transform. In order to obtain the DFT, the Fourier transform of (3.1) has to be sampled by the frequency of T_o. Here, T_o represents the span of windowing function. The frequency sampling function in time domain is given by:

$$\phi(t) = T_o \sum_{k=-\infty}^{\infty} \delta(t - kT_o) \tag{3.2}$$

The multiplication of Fourier Transforms Y(f) and Φ(f) will give the samples in the frequency domain. To obtain the corresponding time domain function $x'(t)$, it is required to convolute between y(t) and ϕ(t).

$$\begin{aligned} x'(t) &= y(t) * \phi(t) \\ &= \left[\sum_{n=0}^{N-1} x(n\Delta T)\delta(t - n\Delta T)\right] * \left[T_o \sum_{k=-\infty}^{\infty} \delta(t - kT_o)\right] \\ &= T_o \sum_{k=-\infty}^{\infty} \left[\sum_{n=0}^{N-1} x(n\Delta T)\delta(t - n\Delta T - kT_o)\right] \end{aligned} \tag{3.3}$$

Here,$x'(t)$ has a period of T_o irrespective of the frequency of input function x(t). Thus, $x'(t)$ is an approximation of x(t). In the case of periodic function, the window length is a crucial part in determining the accuracy Fourier Transform by means of DFT. The Fourier Transform of any signal $x'(t)$ can be written as a sequence of impulse function [17], as shown below.

$$\begin{aligned} X'(f) &= \sum_{k=-\infty}^{\infty} \alpha_k \delta(f - \frac{k}{T_o}), where \\ \alpha_k &= \frac{1}{T_o} \int_{-T_o/2}^{T_o - T_o/2} x'(t) e^{-\frac{j2\pi kt}{T_o}} dt \end{aligned} \tag{3.4}$$

Substituting $x'(t)$ from (3.3) into the expression of α_k. we get,

$$\alpha_k = \frac{1}{T_o} \int_{-T_o/2}^{T_o - T_o/2} \left\{ T_o \sum_{m=-\infty}^{\infty} \left[\sum_{n=0}^{N-1} x(n\Delta T)\delta(t - n\Delta T - mT_o)\right] \right\} e^{-\frac{j2\pi kt}{T_o}} dt \tag{3.5}$$

As the limit on integration is from $-T_o/2$ to $T_o - T_o/2$, which is a period of a signal, we may

use index m when its value is 0 only.

$$\alpha_k = \int_{-T_o/2}^{T_o-T_o/2} \left[\sum_{n=0}^{N-1} x(n\Delta T)\delta(t-n\Delta T)\right] e^{-\frac{j2\pi kt}{T_o}} dt$$

$$or, \alpha_k = \sum_{n=0}^{N-1} \int_{-T_o/2}^{T_o-T_o/2} x(n\Delta T)\delta(t-n\Delta T) e^{-\frac{j2\pi kt}{T_o}} dt$$

$$or, \alpha_k = \sum_{n=0}^{N-1} x(n\Delta T) e^{-\frac{j2\pi kn\Delta T}{T_o}}$$

$$Since, T_o = N * \Delta T, thus$$

$$\alpha_k = \sum_{n=0}^{N-1} x(n\Delta T) e^{-\frac{j2\pi kn}{N}} \tag{3.6}$$

$$where, k = 0, \pm 1, \pm 2, ...$$

The α_k has only N distinct values because α_{N+1} is same as α_1. Hence, $X'(f)$ for each frequency $f = \frac{k}{T_o}$ can be defined as

$$X'(\frac{k}{T_o}) = \sum_{n=0}^{N-1} x(n\Delta T) e^{-\frac{j2\pi kn}{N}} \tag{3.7}$$

$$where, k = 0, 1, 2, ...N-1$$

The Discrete Fourier Transform of N input samples of a signal sampled at an interval of ΔT is defined by (3.7).

3.2 DFT and Phasor Representation

The DFT of a periodic signal can be determined by using the samples of at least 1 cycle. The phasor of a signal represents its RMS magnitude and phase angle. The DFT expression (3.7) should be slightly modified for it to represent the phasor of a periodic signal. The Fourier series coefficients of a signal can be obtained from DFT by dividing the DFT value by N [17]. It is to be noted that the Fourier series coefficient exist for both positive and negative frequencies with equal magnitudes. Thus, the RMS value of the signal can be computed by multiplying the coefficient of any positive frequency by $\sqrt{2}$. The phasor representation of a sinusoidal signal

can be written as:

$$X_k = \frac{\sqrt{2}}{N}\sum_{n=0}^{N-1} x(n\Delta T)e^{-\frac{j2\pi kn}{N}}$$
$$or, X_k = \frac{\sqrt{2}}{N}\sum_{n=0}^{N-1} x(n\Delta T)\left\{cos\left(\frac{2\pi kn}{N}\right) - jsin\left(\frac{2\pi kn}{N}\right)\right\}$$

Defining x(nΔT) = x_n and 2π/N = θ, the above expression can be written as:

$$X_k = \frac{\sqrt{2}}{N}\sum_{n=0}^{N-1} x(n\Delta T)\left\{cos\left(kn\theta\right) - jsin\left(kn\theta\right)\right\} \tag{3.8}$$

This is a required phasor representation of the sinusoidal signal of frequency $f = \frac{k}{T_o}$. The phasor representation of DFT, gives the phase angle with reference to positive peak of the signal as shown in Fig. 3.1. The phasor at any instant could be computed either by taking future sample or by past sample and the angle representation also depends on this criteria as shown in Fig. 3.1.

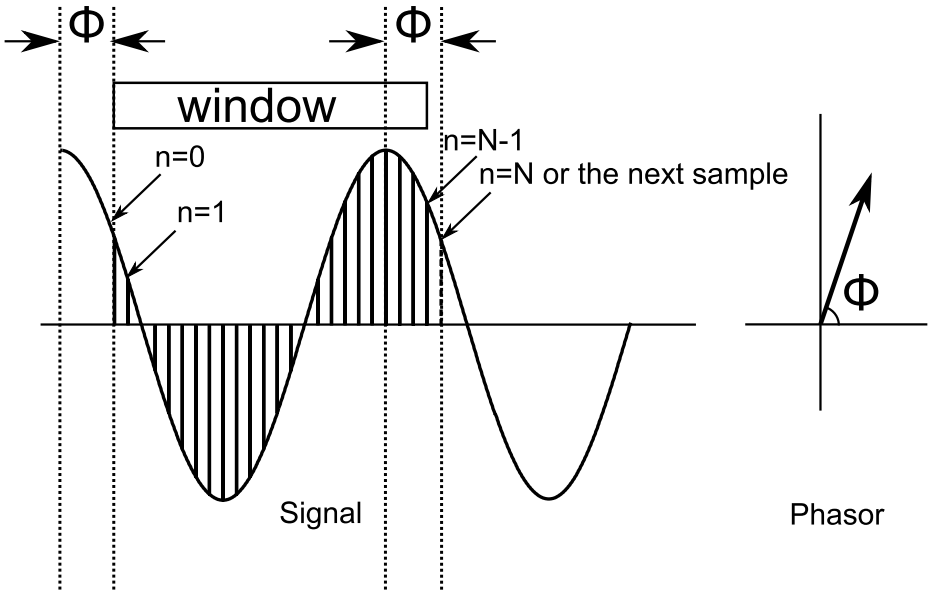

Figure 3.1: Pictorical view of phasor representation by DFT

3.3 Synchrophasor Definition

Synchrophasor representation of the any signal x(t) is differs from the concept of phasor representation (efeq:phasor) in terms of phase angle representation. The phase angle is in synchrophasor is measured relative to the cosine signal at the nominal frequency [20]. The synchrophasor is computed for fundamental frequency ($k = 1$ in (3.8)) of the signal or for

positive sequence component for three phase system.

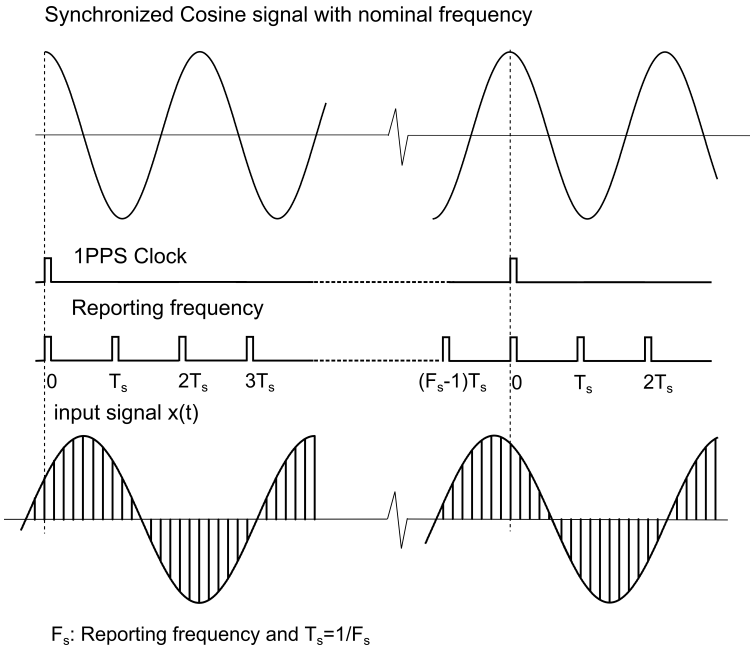

Figure 3.2: Overview of synchrophasor time stamping procedure

A cosine signal of synchrophasor is synchronized such that its positive peak lie at the second rollover of the GPS clock as shown in Fig 3.2. The sampling frequency and reporting frequency are also in synchronous with the GPS clock. The phasor is computed at each reporting instant defined by reporting frequency. Note that, (3.8) needs to be modified according to the definition of synchrophasor, which is shown below.

$$X_1^M = \frac{\sqrt{2}}{N}\left[\sum_{n=0}^{N-1} x(n\Delta T)\left\{cos\left(n\theta\right) - jsin\left(n\theta\right)\right\}\right] e^{-j2\pi f_0 M T_s}$$
$$X_1^M = \frac{\sqrt{2}}{N}\left[\sum_{n=0}^{N-1} x(n\Delta T)\left\{e^{-jn\theta}\right\}\right] e^{-j2\pi f_0 M T_s} \tag{3.9}$$
$$where,\ M = 0,1,2,.....(F_s - 1)$$

The index M is reset at every 1 PPS clock and the angle of the synchrophasor is represented in the range of $-\pi$ to π.

3.4 Accuracy of Phasor Computation vs Window Length

Phasor is defined for static signal. However, in reality, power system is never in steady-state. The voltage and current have drifting fundamental frequency in a narrow range around the

nominal value. Therefore, power systems can be referred as a non-stationary system as there is continuous interactions between power demand, inertia of generators, and automatic speed controllers. Additionally, the faults and switching events makes large and rapid disturbance to power system, causing large deviation of frequency.

In these scenarios, the dynamic phasor estimation using (3.8) is not straight forward. The equation needs the uniform N samples of the signal that lies exactly on a period of signal, which is difficult to meet in dynamic conditions. Mathematically, this condition can be written as:

$$N * \Delta T = T_o \tag{3.10}$$

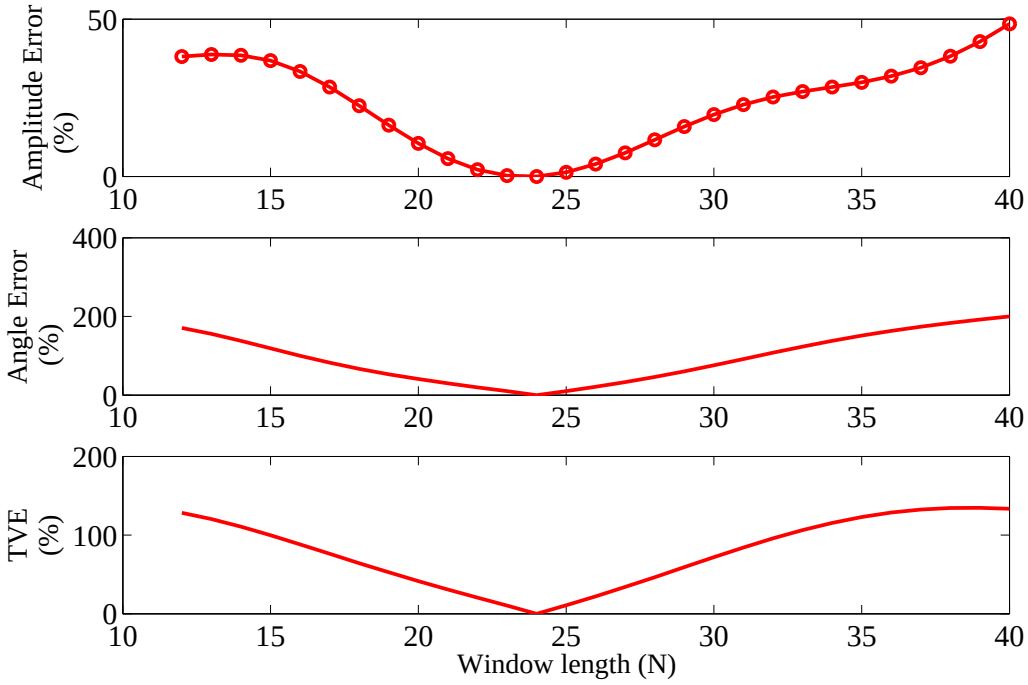

Figure 3.3: Phasor errors vs window length

The error in phasor computation was investigated for different window lengths of the DFT. A sinusoidal signal of 50 Hz was sampled at 24 samples per cycle while the phase angle and amplitude were estimated using (3.8) for various size of window length. The result of this simple test demonstrated that to mitigate the error in phasor computation, the window length should exactly match the time period of the input signal. This is illustrated in Fig. 3.3. In the derivation of DFT equation, the signal is assumed to have a period equal to window length. So, if the window length is not exactly equal to period of signal, the phasor computation by DFT

would be inaccurate. This behavior is illustrated in Fig 3.4. In order to meet this condition, the signal time period (T_o) should be known beforehand. Due to this requirement, the frequency estimation becomes the integral part of phasor estimation. If the condition outlined in (3.10) is not satisfied, it leads to signal discontinuity at window edges. This would result to spectral leakages, and finally spurious phasor calculation. This condition could be met by following strategies:

1. Varying N
2. Varying sampling time (ΔT)
3. Varying sample values or by interpolation

The sliding window DFT along with one of these strategies could be applied for continuous phasor estimation. The pros and cons of each technique is described in literature review in section 2.5.2.

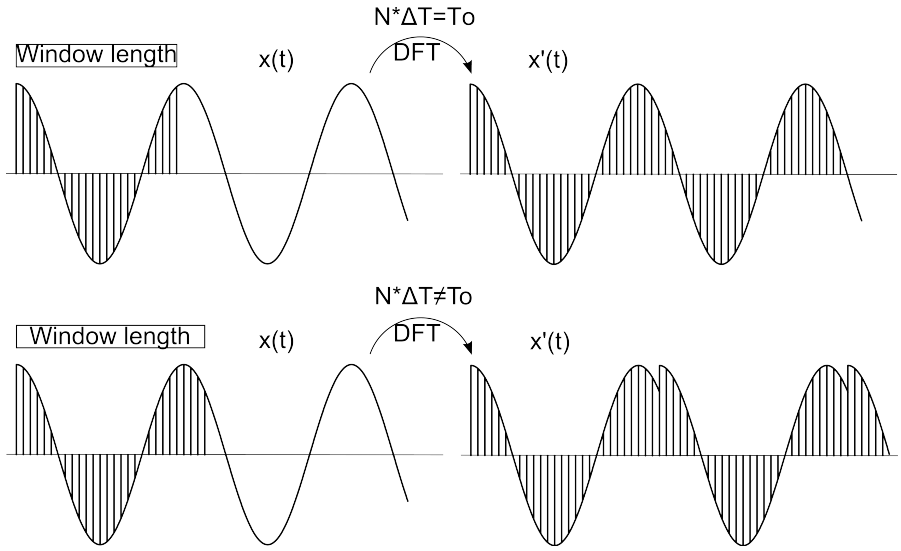

Figure 3.4: Improper window length results in signal discontinuity at edges of window

3.5 Conventional Approach of Phasor Computation: Enhanced DFT

The signal discontinuity at the edges of window at off-nominal frequencies result in inaccurate DFT computation. Additionally, in single phase application, DFT estimation suffers from second harmonic oscillation in phase angle and amplitude estimation [17]. In enhanced DFT, a

three point average filter is employed to mitigate the second harmonic oscillation and finally a correction factor compensates the error due to off-nominal frequency as shown in Fig. 3.5. Such correction factor is dependent on frequency of the input signal. Hence, a frequency estimator becomes an integral part of enhanced DFT. The correction factor P is calculated as:

$$P = \left\{ \frac{sin\frac{N(\omega-\omega_o)\Delta T}{2}}{Nsin\frac{(\omega-\omega_o)\Delta T}{2}} \right\} e^{j(N-1)\frac{N(\omega-\omega_o)\Delta T}{2}} \tag{3.11}$$

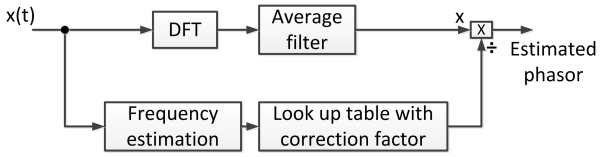

Figure 3.5: Benchmark algorithm for phasor estimation

For mitigation of second harmonic oscillation, the three-point average filter for $N = 24$ sample per cycle DFT is given by:

$$y(k) = \frac{1}{3}(u(k) + u(k-4) + u(k-8)) \tag{3.12}$$

The average filter also shifts the phase of signal which also need to be compensated. The gain of three point average filter is calculated as: The three point average filter is:

$$y(k) = \frac{1}{3}(u(k) + u(k-4) + u(k-8))$$
$$or, y(k\Delta T) = \frac{1}{3}[u(k\Delta T) + u\{(k-4)\Delta T\} + u\{(k-8)\Delta T\}]$$

Taking the Laplace Transform and substituting $s = j\Delta\omega$, we get.

$$\frac{Y(j\omega)}{U(j\omega)} = \frac{1}{3}(1 + e^{-4j\Delta T\Delta\omega} + e^{-8j\Delta T\Delta\omega})$$

The gain is complex and frequency dependent. For instance, lets take the test signal of frequency 45 Hz where the enhance DFT is designed for nominal frequency of 50 Hz. Thus the correction factor for this signal for the DFT with $N = 24$ and $\Delta T = 833.333\mu s$ would be P=0.98365$\angle$ -17.24°. Similarly, the average filter gain for -5 Hz frequency deviated signal would be 0.99635$\angle$5.999°.

3.6 Time clock Synchronization and Measurements

As noted in early sections, the magnitude and frequency of a node voltage in the power grid is non-stationary. Also, the phase angle varies from -π to π per cycle in every oscillating signal. It is more significant to compare phase angle, magnitude, and frequency between two nodes in the power grid. Hence, measuring units placed at different locations need to be time synchronized so that the measurements made at same instant could be identified and compared. Additionally, the time-synchronized measurements in the power system could give a snapshot of the grid at every measurement instants. This makes the PMUs suitable for wide area monitoring system (WAMS). Usually, the GPS clock is used for time synchronization because of its availability all over the network and has timing accuracy of 100 nanoseconds [38]. The GPS receivers at any location can generate highly accurate 1 PPS clock, which are synchronous to one another. This clock has to be divided into small segment of time which is either done by sampling frequency or by internal clock. The division of the 1 PPS is dependent on the reporting rate of the PMU. In other words, the internal clocks of PMU should have a frequency equal to the reporting rate and be in synchronous with 1 PPS. The synchronization in PMU is of utmost importance for time synchronized measurements. The method of internal clock synchronization used in this research is presented in Fig. 3.6.

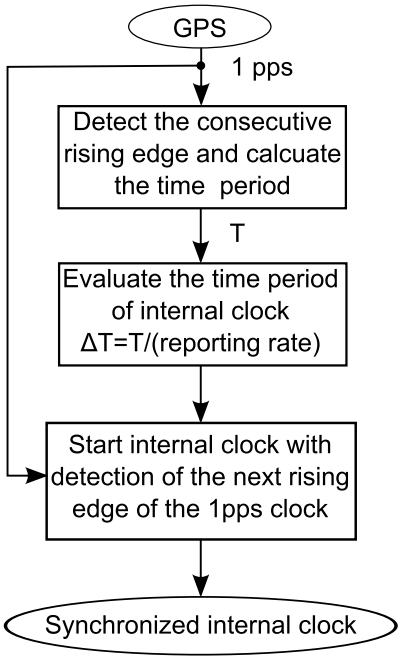

Figure 3.6: Timing synchronization process diagram

The measurements of the signal was done at each rising edge of the internal clock.

3.7 Proposed Method 1: Discrete Fourier Transformation with Variable Sampling Time

As described in section 3.1, that the accuracy of dynamic phasor estimation by DFT depends upon the validity of (3.10) at each step of computation. In this method, a variable sampling time approach was implemented to increase the accuracy of estimation under large variation of system frequency.

A PMU measures the phasor with reference to a synchronized clock. Usually, a constant sampling time is synchronized with 1 PPS clock for segmenting the time into multiple euqal intervals. Measurements are subsequently taken at each instant of the interval. In contrary, this section describes a new synchronizing method and novel system for phasor estimation by using variable sampling time.

It was already highlighted in [17] that keeping the time-tag with variable sampling time approach would be difficult because each instant of measurement had to recalculated from a reference time by summing the sampling periods. This will require a separate memory to store the sampling period of each samples and calculate the time tag information. A new of generating synchronized measurements with easy time-tagging method is proposed in this method. The Fig. 3.7 shows the design of PMU based on VST approach.

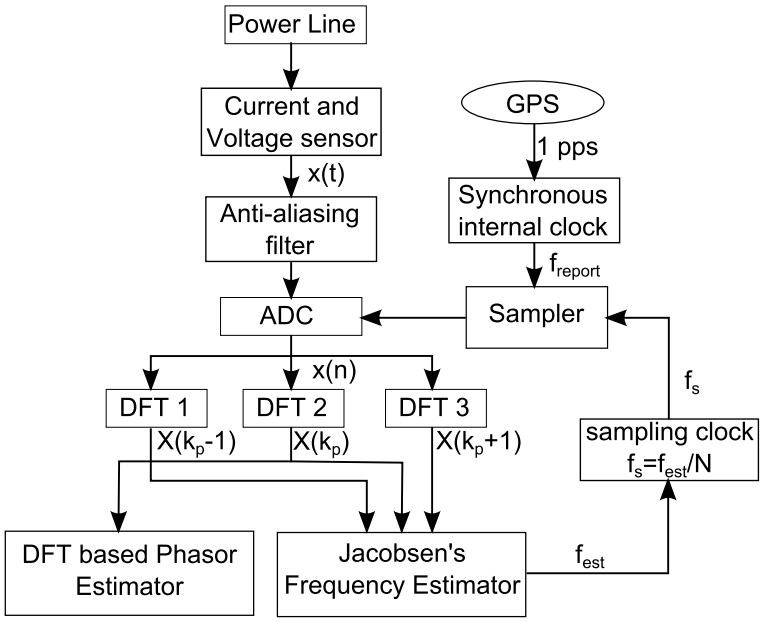

Figure 3.7: Proposed phasor measurement unit using variable sampling strategy

The proposed system used hybrid form of sampling. The sampling time was fixed within

window length but could be different for the consecutive window length. The sampling time is adjusted in real time depending on the singal frequency. Now, for time tagging this system used an extra internal clock that was synchronized with the 1 PPS clock. Moreover, the internal clock kept the timing information and hence the time tagging challenge was solved without summing the sampling time.

The phasor calculation is dependent on the instant of estimation. So, the system used the rising edge of the internal clock as the instant at which the phasor was estimated. The frequency of internal clock defined the reporting rate for this system. The sampler would be activated simultaneously by the rising edge of the internal clock and the sampled at the rate which was N times the previously estimated system frequency ($f_s = N * f_{sys}$). The sampler would take only N samples and stopped. The analog to digital converter transformed the analog signal to digital form, which were stored in a array. This array of digital signal was used to compute the phasor by utilizing DFT. Since the frequency of the system had to be known, a frequency estimator was deployed to correct the sampling time. As a result, the phasor was computed continuously.

Bias corrected Jacobsen was implemented in this system for frequency estimation. This technique required three DFT points to estimate the true frequency of signal. The digital signal stored in array in each instant of phasor computation were utilized to compute the DFT at three different frequency bins, which were needed for frequency estimation. The mid frequency bin is always close to the real system frequency and was used for phasor estimation. The precise estimation of frequency could aid in tuning the sampling frequency of the sampler, which ensured the condition of (3.10) was met. This sampling time correction loop ensured the accuracy of the DFT, and eventually the frequency and phasor estimations.

3.7.1 Phasor Estimation

The phasor estimation utilized (3.8) for phasor extraction from the signal. However, utilization of this equation needed to ensure that the window length is tuned to the signal time period at every instant of calculation. The tuning of window length is done dynamically by adjusting the sampling time of the sampler. As explained in the earlier section, the internal clock is synchronized with the 1 PPS clock of the GPS for time stamping the instant of phasor measurement. The rising edge of the internal clock initiates the sampler and ADC. They will convert N samples into digital form and stops until the next rising edge of the internal clock. The number of samples per cycle (N) was fixed in this system.

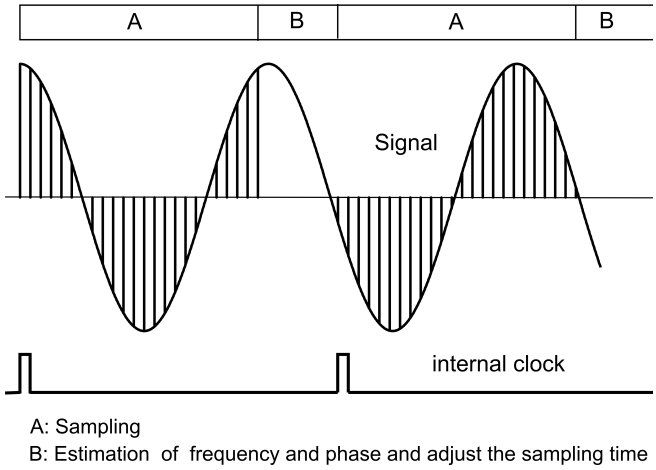

Figure 3.8: Proposed methodology for phasor estimation

In Fig. 3.8 the sampling duration is indicated by a period A. The remaining time until the next rising edge of the internal clock is indicated by B. At period B, the calculation of phasor and frequency is performed with the sampled signal. The estimated frequency also help to adjust the sampling time for the next sampling period A. This adjustment will ensure that the window length is exactly equal to the time period of the signal and discontinuity at edges due to rectangular window is highly reduced. This also ensured the phasor estimation is accurately performed. The maximum reporting rate this method can generate is equal to the system frequency.

3.7.2 Frequency Estimation

The frequency of a signal cannot be directly measured. It is generally estimated because the signal is usually corrupted with noise and harmonics in power systems. The frequency estimator utilizing the zero crossing detector are simple to implement, but the accuracy is degraded with noise. DFT is used commonly for estimation of frequency since they can filter out noise and harmonics. Theoretically, the frequency at which the global maximum of the spectrum occurs is the signal frequency. DFT can be utilized to obtain the discrete frequency spectrum of signal. Based upon the phasor and corresponding frequency bins, the frequency of the signal can be precisely estimated. First a coarse search is executed by large stepping of frequency bins to get the rough estimation of signal frequency, then a fine search is implemented with smaller steps of bins around the vicinity of the frequency obtained in first stage. Referring to [39], the two-stage search improved the frequency estimation.

In the literature, the second stage search has been done by utilizing the function of DFT

samples, instead of searching by stepping the frequency bins. The algorithms proposed in [40, 41, 42] used three-point DFTs, whereas [43] utilized only two DFT samples for fine estimation of frequency. Another three-point DFT method was proposed by Jacobsen in [44], which was able give more accurate frequency under wide range of signal to noise ratio (SNR). The empirical relation of [44] was verified mathematically in [45]. It also proposed a bias correction term to improve the accuracy of estimation for small sample window.

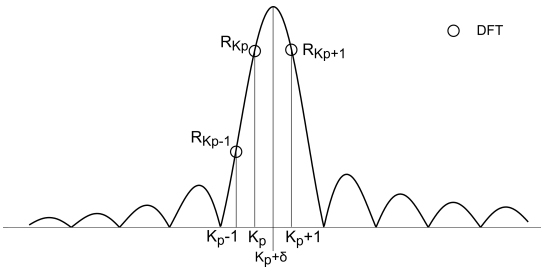

Figure 3.9: Magnitude spectrum of signal with central frequency bin at $K_{p+\delta}$.

Jacobsen's expression works fine for a single tone frequency estimation corrupted with noise. However, it cannot be used directly in power system as the frequency of the grid is not stationary. Since DFT is a frequency dependent filter, the window length has to be corrected at every DFT to ensure correct computation, especially when using a small rectangular window.

In power systems, the grid frequency is roughly known. Thus, a coarse search is not needed. The approximate location of the frequency bins (k_p) around the actual frequency could be predicted. With extra two frequency bins (k_p-1 and k_p+1), the location of the actual frequency can be estimated by calculating the δ. Fig. 3.9 illustrates the principal of frequency estimation used in this paper. The calculation of δ can be done by various techniques shown in Table 3.1.

Table 3.1: Different Methods for Estimation of δ

FFTMLE	fine and coarse search by stepping the frequency bins
Parabolic	$\delta = \frac{\lvert R_{kp+1}\rvert - \lvert R_{kp-1}\rvert}{4\lvert R_{kp}\rvert - 2\lvert R_{kp-1}\rvert - 2\lvert R_{kp+1}\rvert}$
Quinn	$\alpha_1 = Real(\frac{R_{kp-1}}{R_{kp}}), \alpha_2 = Real(\frac{R_{kp+1}}{R_{kp}})$ $\delta_1 = \frac{\alpha_1}{1-\alpha_1}, \delta_2 = \frac{\alpha_2}{1-\alpha_2}$ if $\delta_1 > 0$ and $\delta_2 > 0$, $\delta = \delta_2$ else $\delta = \delta_1$
MacLeod	$d = \frac{Real(R_{kp-1}R^*_{kp} - R_{kp+1}R^*_{kp}}{Real(2\lvert R_{kp}\rvert^2 + R_{kp-1}R^*_{kp} + R_{kp+1}R^*_{kp})}$ $\delta = \frac{\sqrt{1+8d^2}-1}{4d}$
Jacobsen	$\delta = Real(\frac{R_{kp-1} - R_{kp+1}}{2R_{kp} - R_{kp-1} - R_{kp+1}})$
Bias corrected Jacobsen	$\delta = \frac{tan(\pi/N)}{N} Real(\frac{R_{kp-1} - R_{kp+1}}{2R_{kp} - R_{kp-1} - R_{kp+1}})$

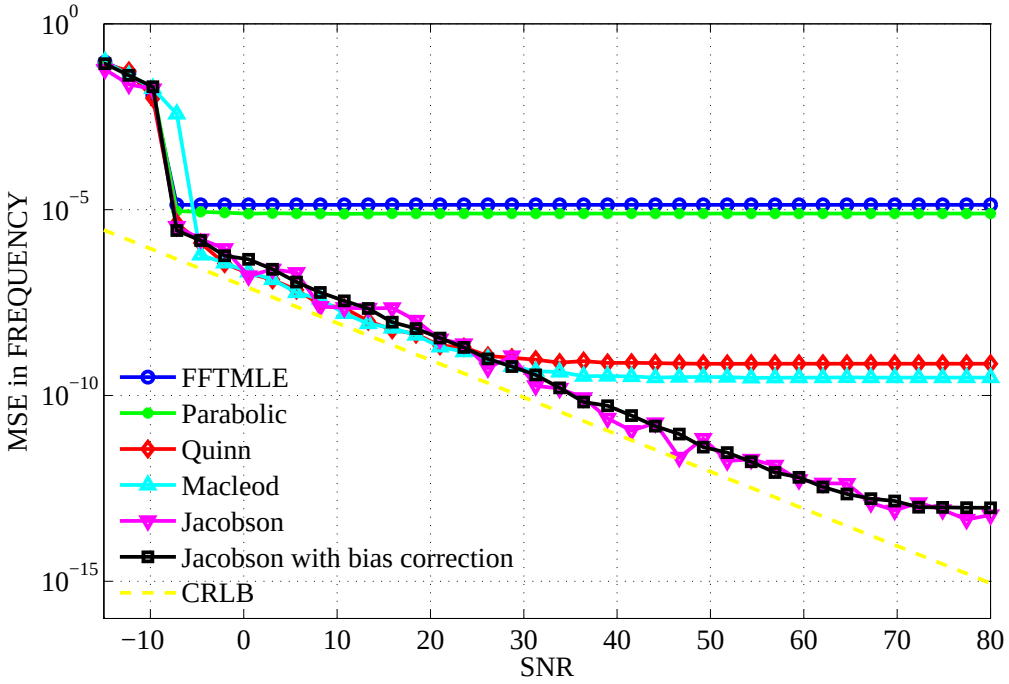

Figure 3.10: Comparison between various 3 point DFT frequency estimator

CramrRao lower bound (CRLB) was used as the benchmark for the performance of the estimator. The lower bound of the mean square error on frequency estimation depends on the number of samples used. The minimum variance of the frequency estimation of a given signal could be described by (3.13) as noted in [46].

Fig. 3.10 presents performance of various 3 point DFT algorithm listed in Table 3.1. The biased Jacobsens method demonstrated to be an efficient estimator since it was closest to CRLB for signals over a wide range of Signal to noise ratio (SNR). Hence, the method has been used for frequency estimation in this proposed technique.

$$var(f) = \frac{12\sigma^2}{b_o^2 T_s^2 N_t (N_t^2 - 1)} \tag{3.13}$$

where,

b_o = amplitude of signal

N_t = total samples

T_s = sampling time

3.7.3 Real-Time Rate of Change of Frequency Estimation

If f_i is the frequency of the signal estimated at the instant of $i = 0,1,2,3...,N-1$, then the rate of chage of frequency is given by [51]:

$$ROCOF = \sum_{i=0}^{N-1} \beta_i f_i \tag{3.14}$$

where,

$$\beta_i = \frac{12i - 6(N-1)}{N(N^2-1)}$$

3.8 Proposed Method 2: Discrete Fourier Transformation by Sample Value Adjustment

3.8.1 Phasor Estimation

In this method, SVA is introduced as pre-DFT signal interpolator, which transform the input signal of any frequency to system frequency. The merit of SVA is that it mitigates drawback of DFT at off-nominal frequencies with fair computational complexity.

A. Background

Sample value adjustment (SVA) is a technique to transform the input signal of any frequency to the standard frequency. With minor computation burden, SVA can efficiently transform the frequency of signal compared to over-sampling and re-sampling technique. It is an interpolation technique which need to have frequency information of the incoming signal. Thus, frequency of input signal also need to estimated in order to make real time computation. In practical application, the signal is stored in digital form in buffers of the signal processor. Since, single cycle DFT is the main concern of study, the SVA adjustment was made for data length of one cycle. The range of frequency of input signal under interest was from $45Hz$ to $55Hz$. The buffer length was selected for the longest time period of signal. If the nominal window length is N, then the longest window length required could be determined as in (3.15).

$$m \geq N * \frac{f_o}{f_{min}} \tag{3.15}$$

where, f_{min} is minimum and f_o is nominal frequency.

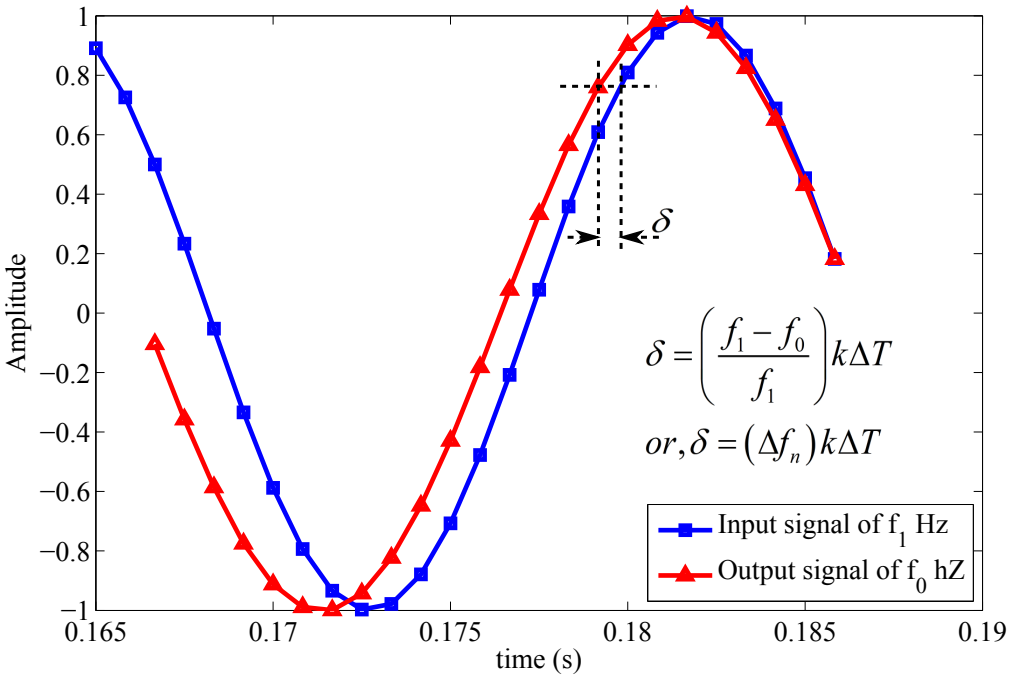

Figure 3.11: Relation between the sample values of signals with same amplitude but different frequency

For instance, if $f_o = 50Hz$ and $N = 24$, then the maximum buffer length would be $m >= 24 * 50/45 \approx 26$. After then, a spline interpolation was employed for recalculation of sample values from the buffer, utilizing the first and second derivatives as in (3.17),(3.18). The sample values of the nominal signal can be determined from that of the input signal, by calculating displacement (δ) for each samples, from a neighboring reference sample value. The relation for δ for each samples is shown in Fig. 3.11. Then a Taylor series upto third term was used to find the new sample values of the output signal. Since, the output signal is designed to have a nominal frequency, DFT was also designed for the same frequency. Hence, the output of DFT would have minimum signal discontinuity which ascertain the accuracy of the phasor estimation. The similar appraoch was also presented in [33], but it used first order approximation.

B. Algorithm Development

The algorithm uses the notation x and y for the input sampled signal and for output signal. x_0 represents the recent sample at time t_0. k and h denotes the sample index and sampling interval. The recent sample remained unchanged, i.e $y_0 = x_0$, while the older samples in the buffer would be adjusted by spline interpolation. The adjustment would depend on the frequency deviation

from nominal value i.e, $\hat{f} - f_0$ and the normalized frequency deviation is calculated as:

$$\triangle f_n = \mid \frac{\hat{f} - f_0}{\hat{f}} \mid \tag{3.16}$$

where $\hat{f}$ is the estimated frequency and the estimation technique of it is explained in section III. The first and second derivatives for spline interpolation are calculated as:

$$\frac{dx_k}{dt} = \frac{1.5x_k - 2x_{k-1} + 0.5x_{k-2}}{h} \tag{3.17}$$

$$\frac{d^2x_k}{dt^2} = \frac{x_k - 2x_{k-1} + x_{k-2}}{h^2} \tag{3.18}$$

1) For under and nominal frequency signal, the output values y_k for k=-1, -2, ... $-N-1$ are calculated as:

$$y_k = x_k + \frac{dx_k}{dt}\alpha h + \frac{d^2x_k}{dt^2}\frac{(\alpha h)^2}{2} \tag{3.19}$$

where α is

$$\alpha = k * \triangle f_n$$

Substituting (3.17) and (3.18) in (3.19), we get,

$$y_k = b_0 x_k + b_{-1}x_{k-1} + b_{-2}x_{k-2} \tag{3.20}$$

where,

$$b_0 = 1 + 1.5\alpha + 0.5\alpha^2$$

$$b_{-1} = -\alpha(2 + \alpha)$$

$$b_{-2} = 0.5\alpha(1 + \alpha)$$

2) For over frequency signal, the output values y_k for k=-1, -2, ... $-N-1$ are computed as:

$$y_k = x_{k+1} + \frac{dx_{k+1}}{dt}\beta h + \frac{d^2x_{k+1}}{dt^2}\frac{(\beta h)^2}{2} \tag{3.21}$$

where β is

$$\beta = -1 - k * \triangle f_n$$

Again, substituting (3.17) and (3.18) in (3.21), we get,

$$y_k = b_1 x_{k+1} + b_0 x_k + b_{-1} x_{k-1} \tag{3.22}$$

where,

$$b_1 = 1 + 1.5\beta + 0.5\beta^2$$

$$b_0 = -\beta(2+\beta)$$

$$b_{-1} = 0.5\beta(1+\beta)$$

The output signal y, stored in an output buffer would have constant sample per cycle and sampling time. Hence, DFT could be applied to compute the instantaneous phasor of the input signal.

3.8.2 Frequency Estimation

The SVA algorithm is incomplete with frequency information of the input signal, which is not known in real-time. This section describes about the frequency estimation in real-time to assist the proposed algorithm.

A. Background

In literature, different approaches had been implemented for tracking the power system frequency [47, 48, 49]. The simplest one is computing the time period of signal using zero crossing detection method. Although zero crossing detection is simple to implement, this algorithm is not immune to noise and estimation rate is slower. A modified zero crossing along with DFT polynomial fitting by least square method was implemented in [47] for estimating frequency. In the same paper, the another method of frequency estimation by phase demodulation technique was presented which needed arctan function for frequency calculation. The disadvantage of using the least mean square technique is the large computational burden and slow convergence rate. Similarly, arctan function is a time consuming operation not suitable for real time frequency estimation. In this paper, the frequency estimation using only three consecutive sample value of the input signal has been proposed. The similar approach was mathematically derived in [48, 49] using least square approach and variance minimization technique. In comparison, the least square technique is easier to apply and understand.

The purpose frequency estimator implements Recursive Least Square (RLS) algorithm

instead of Least square method because of faster computation and similar performance. The conceptual design of frequency estimator is similar to one described in [48]. It uses nine samples divided into 3 section to find out three different frequency and finally average them to get the signal frequency, where as the purposed method only used three sample to find out the frequency and the performance of both was found to be same.

B. Algorithm Development

Lets consider the voltage signal sampled uniformly with sampling time T_s as:

$$v(n) = Acos(\omega t_n + \phi_0) = Acos(\omega n T_s + \phi_0) \tag{3.23}$$

$$where, \omega = angular frequency = 2pi * f$$

$$\phi_0 = initial phase$$

$$A = amplitude$$

$$Similary,$$

$$v(n-1) = Acos(\omega(n-1)T_s + \phi_0)$$

$$v(n+1) = Acos(\omega(n+1)T_s + \phi_0)$$

$$Then,$$

$$v(n-1) + v(n+1) = 2Acos(\omega n T_s + \phi_0)cos(\omega T_s) = 2v(n)cos(\omega T_s) = \eta v(n) \tag{3.24}$$

$$where, \eta = 2cos(\omega T_s) = \frac{v(n-1) + v(n+1)}{v(n)}$$

Then the actual frequency f is estimated as

$$\hat{f} = \frac{arccos(\eta/2)}{2\pi T_s} \tag{3.25}$$

The frequency estimated by (3.25) do not take noise into consideration, so a low pass filter should always be used with this algorithm. The direct use of (3.25) has two drawback for implementation. The first demerit is that, when $v(n)$ is zero η approach to infinity and frequency cannot be computed [50]. Therefore, recursive least squares (RLS) algorithm can be applied to (3.24) for estimation of η. Using, the estimated value of η in (3.25) eliminates the first demerit.

The process of estimation of η is shown below:

$$\text{Initialization:} \eta(1) = 0,\ P(1) = \delta$$

Computation for n=2,3,....

$$\begin{aligned} k(n) &= \frac{P(n-1)v(n)}{\lambda + v^2(n)P(n-1)} \\ \xi(n) &= v(n) + v(n-2) - \eta(n-1)v(n) \\ \eta(n) &= \eta(n-1) + k(n)\xi(n) \\ P(n) &= \lambda^{-1}P(n-1) - \lambda^{-1}k(n)v(n)P(n-1) \end{aligned} \tag{3.26}$$

Here, λ is a forgetting factor and δ is an initial value of variance (P).

The second demerit of (3.25) for implementation in DSP is that it uses arccosine operator, which is a time consuming operation. For real-time estimation, the computation time has to be reduced. As a result, arccosine term is eliminated by rewriting (3.24) in terms of frequency deviation ($\triangle\omega$) from nominal frequency (ω_0), which is shown below:

$$\begin{aligned} v(n-1) + v(n+1) &= 2v(n)cos(\omega T_s) = 2v(n)cos((\omega_0 + \triangle w)T_s) \\ &= 2v(n)cos(\omega_0 T_s)cos(\triangle\omega T_s) - 2v(n)sin(\omega_0 T_s)sin(\triangle\omega T_s) \end{aligned} \tag{3.27}$$

In power systems, the frequency deviation is small and the sampling time is also small. Thus we can neglect the term $\triangle\omega T_s$ in (3.27) and rewrite it using the relation $\omega_0 = 2\pi f_0$, $T_s = 1/f_s$, $\triangle\omega = 2\pi \triangle f$ and $f_s = Nf_0$, we get,

$$\begin{aligned} \triangle f &= \frac{2cos(\frac{2\pi}{N})v(n) - v(n+1) - v(n-1)}{4\pi T_s sin(\frac{2\pi}{N})v(n)} \\ or, \triangle f &= \frac{2cos(\frac{2\pi}{N}) - \eta}{4\pi T_s sin(\frac{2\pi}{N})} \end{aligned} \tag{3.28}$$

The estimated value of η from RLS can be applied to (3.28) to get the frequency deviation and finally the estimated frequency is

$$f(n) = f_0 + \triangle f(n) \tag{3.29}$$

Lastly, the ROCOF estimation was performed using the same slope filtering technique, explained in Sec. 3.7.3.

3.9 Enhanced DFT vs Proposed Method

The phasor estimation using enhanced DFT and proposed method 2 is compared in this section. Both SVA and enhanced DFT implement constant sampling frequency approach and the final estimation from them can be compared easily. Whereas, the VST utilizes variable sampling frequency and has smaller reporting frequency, due to which estimation from it cannot be directly compared with enhanced DFT. The test signal used for this comparative study is shown below.

$$x(t) = \sqrt{2}cos(2\pi f_1 t) \tag{3.30}$$
$$where,\ f_1 = 45\ Hz$$

The R.M.S value of signal $x(t)$ is 1 where as frequency deviation is $\Delta f = -5Hz$. The theoretical phase angle with respect to rotating phasor at nominal frequency($f_o = 50Hz$) would be as shown below.

$$\phi(t) = 2\pi\Delta f t$$
$$or, \phi(t) = -10\pi t \tag{3.31}$$

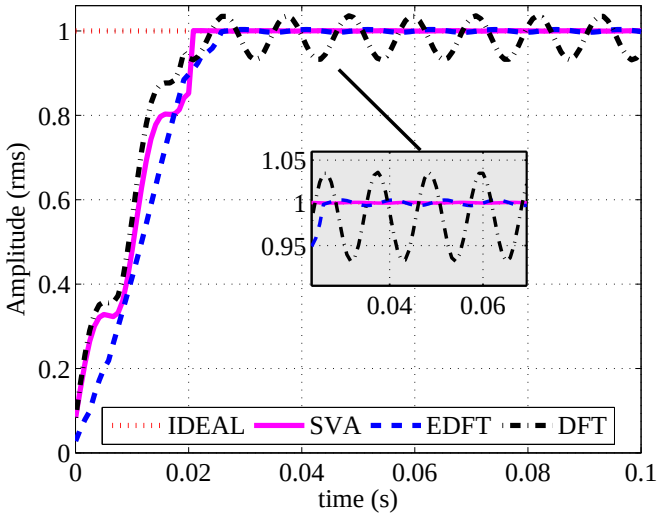

Figure 3.12: Amplitude estimation using various approaches

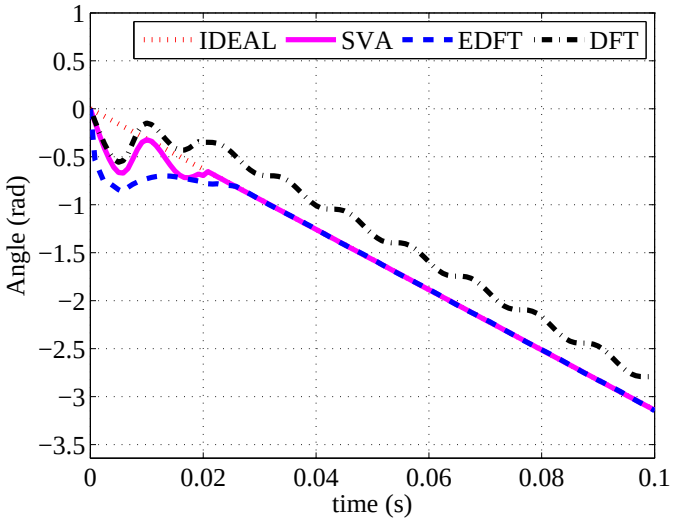

Figure 3.13: Phase angle estimation using various approaches

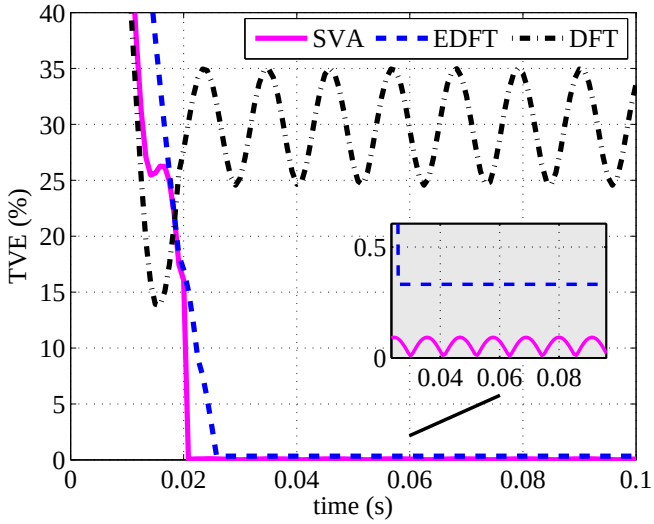

Figure 3.14: Comparison of TVE from different phasor estimation approaches

With $N = 24$ and $\Delta T = 833.333\mu s$, the phasor of signal (3.30), was extracted by means of simple DFT, enhanced DFT and by proposed method2. For this comparative offline study, the frequency estimator was not taken into consideration rather assumed to be known. The estimation of amplitude and phase angle is shown in Fig. 3.12 and 3.13. Estimation from simple DFT has higher second harmonic oscillation in estimated amplitude and phase angle. The phase angle estimated from simple DFT has an offset and the value of offset depends on the frequency deviation of the input signal. The TVE from simple DFT is 25% for this test signal, which is not acceptable. The enhanced DFT was able to reduce the oscillation in estimations including offset in angle estimation. By use of enhanced DFT, TVE became less than 1%, which is under

the compliance. The demerit of enhanced DFT in real time estimation is that, complexity in calculation of correction factor and phase correction due to average filter. The proposed SVA performed superior than the enhanced DFT in terms of both accuracy and faster convergence. The proposed SVA was able to reduced the TVE by more than half that from enhanced DFT. The convergence of estimation also became faster with SVA. The SVA require 1 cycle time of the signal for convergence where as for enhanced DFT, it is slighter higher than 1 cycle time period as shown in Fig. 3.12, 3.13, and 3.14.

CHAPTER 4

Results and Discussions

The proposed methods for real-time phasor computation, described in Chapter 3, were tested with various types of input test signals and their performance indexes were checked to comply with IEEE Standard C37.118.1. This section illustrates the performance of the simulation model of PMU developed with the proposed methods. Futhermore, the experimental setup is described and the process of PMU data validation for proposed method 2 is shown in details. Finally, the result analysis and comparison are discussed.

4.1 Simulation Result of Proposed Method 1

The proposed method is a window tuning algorithm for phasor computation using DFT. In this method N is fixed and ΔT is tuned according to signal frequency. The MATLAB model of PMU utilizing this method used $N = 24$ and reporting rate of $F_r = 20Hz$. The performance of this method is shown in following section at steady-sate and dynamic conditions. As the sampling frequency cannot be synchronized with the 1 PPS clock from GPS, additional internal clock has to be synchronized for easy time tagging of the measurements. The internal clock also indicates the instant of the measurement to be made. Hence, in the simulation plots, the beads in the plot represent the acutal measurement and the beads have been joined by lines just for visualization.

4.1.1 Steady State Test

The input signal of various frequencies between $45Hz$ to $50Hz$ were used to check the performance of the system at steady-state. Fig. 4.1 depicts the performance the purposed algorithm for two different signal. The signal 1 was normal sinusoid of rms value 1 and frequency 53 Hz, where as signal 2 was with 5% 2^{nd} harmonics and 10% 3^{rd} harmonics. For both type of input signal, the TVE is less than 1%, which comply with the standard. Similarly, Fig. 4.2 and 4.3 presents the performance of the proposed method at various range of off-nominal frequency. It was determined that TVE was less than 1% for all input signals at nominal and off-nominal frequencies. The synchrophasor rotates at higher speed at large off-nominal frequency, which is indicated form the angle estimation in Fig. 4.2 and 4.3. At nominal frequency the synchrophasor is in phase with the phasor of internal cosine signal, as a result the angle estimation is always 0.

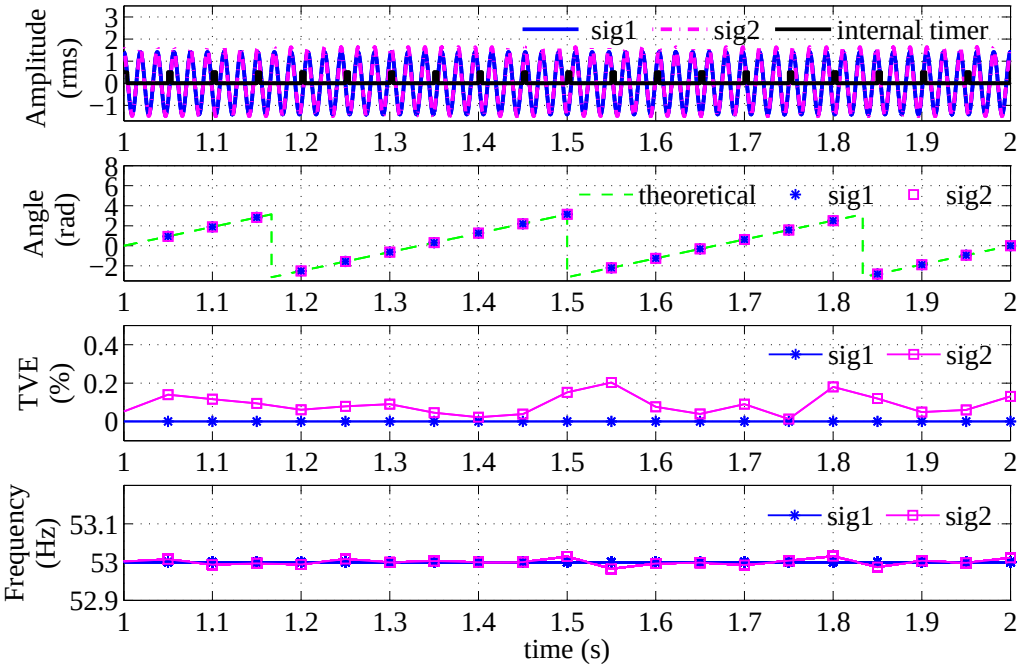

Figure 4.1: Sig 1: normal sinusoid at 53 Hz and sig 2: normal sinusoid at 53 Hz with 5% 2^{nd} and 10% 3^{rd} harmonics. Performance under nominal and distorted signal

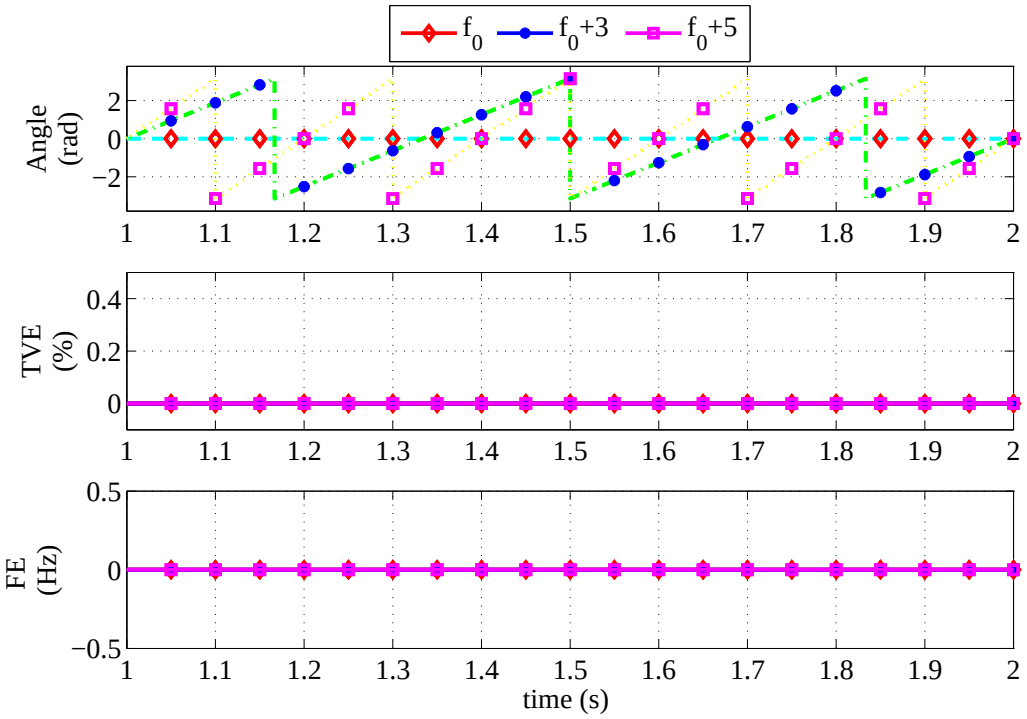

Figure 4.2: Performance of PMU under off-nominal frequencies f_0, f_0+3 and f_0+5 Hz, where f_0=50 Hz.

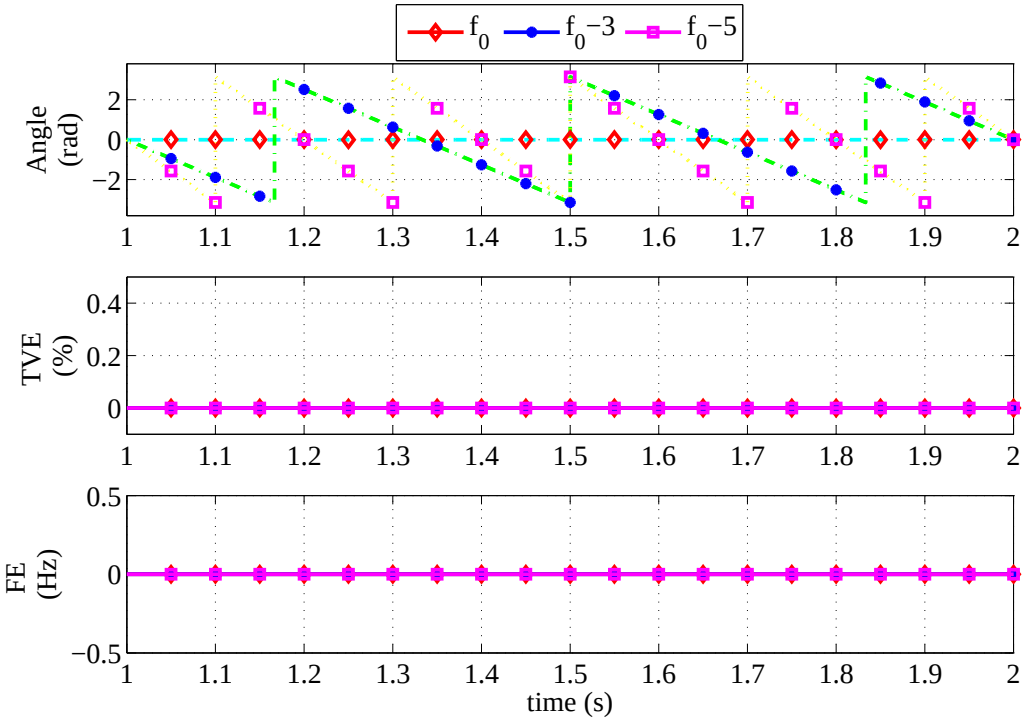

Figure 4.3: Performance of PMU under off-nominal frequency f_0, f_0-3 and f_0-5 Hz, where f_0=50 Hz.

4.1.2 Dynamic Test

A. Ramp Frequency Test

The test signal used for this ramp frequency test was:

$$x(t) = A\cos(2\pi f_0 t + \pi R_f t^2) \tag{4.1}$$

where,

$$A = \sqrt{2},$$

$$R_f = \text{ramp rate}$$

For ramp frequency test, the nominal signal was ramped at $t = 1s$ with maximum of $1Hz/s$. The estimation result shown in 4.4, had TVE less than 1% for entire ramping time. Before the ramp, the TVe was nearly 0 but after ramping TVE slightly increased to 0.6%, which is under compliance. Thus the synchrophasor rotated in a parabolic manner as shown angle estimation subplot of Fig 4.4. Furthermore, Fig. 4.5 presents the estimation made for various ramp rates ranging form $-1Hz/s$ to $1Hz/s$ and for this entire ramp rate, the TVE is less than 1%. The frequency and rate of change of frequency is following the signal, which can be seen from the subplots 2 and 3 of Fig. 4.5. Finally, Fig. 4.6, depicts the frequency and rate of change of frequency error. The FE increases with higher value of ramp rate, where as RFE peaks only at the instant of ramping and decays faster to 0 with time. The FE for ramp rate of $1Hz/s$ and $-1Hz/s$ was slightly higher than the maximum allowed value by the standard (0.01 Hz) but was able to follow due to which the TVE is less than 1%.

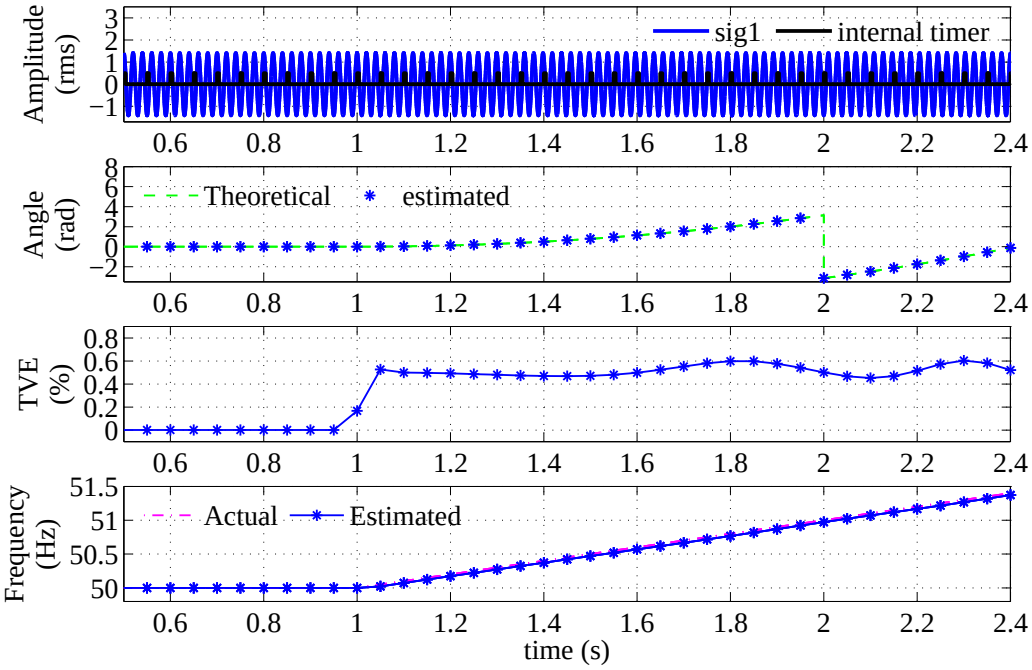

Figure 4.4: sig1 of 50 Hz subjected to ramp of 1 Hz/s at t = 1sec. Performance before and during the ramp frequency test.

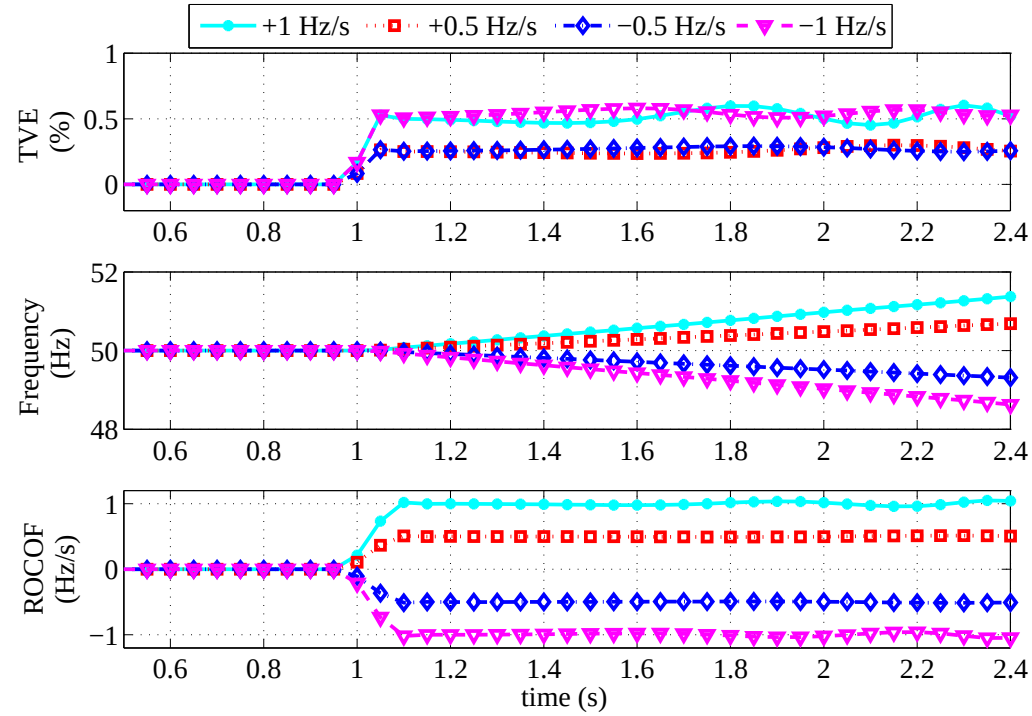

Figure 4.5: Performance at various ramp rate starting at $t = 1sec$.

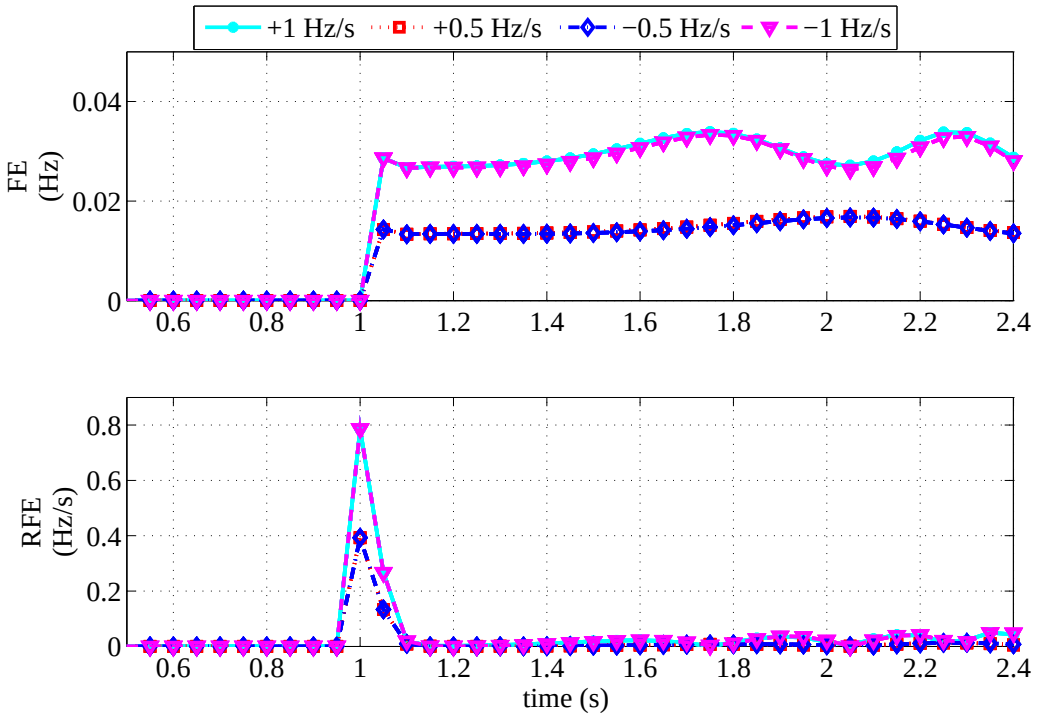

Figure 4.6: Error calculation at different ramp rates of frequency starting at $t = 1sec$.

B. Modulated Signal Test

The test signal used for this test was:

$$x(t) = A[1 + k_x cos(2\pi f_m t)]cos[2\pi f_0 t + k_a cos(2\pi f_m t)] \tag{4.2}$$

where,

$A = \sqrt{2}$, $k_x =$ amplitude modulation factor

$k_a =$ angle modulation factor, $f_m =$ modulation frequency in Hz

As per the standard, amplitude and phase modulation factor of 0.1 and maximum modulation frequency of $2Hz$ was used in the test signal. The estimation result from this proposed algorithm shows that it is following signal amplitude, phase, frequency, and ROCOF despite small delay is there in frequency and ROCOF estimation, as shown in Fig. 4.7. Fig. 4.8, shows that the TVE is less than 3%, which is in compliance with the standard. The maximum frequency error for this modulation is nearly $0.06Hz$, which is just equal to maximum allowed FE ($0.06Hz$) by the standard. Finally, the RFE is less than $1Hz/s$, which is less than maximum allowed RFE ($3Hz/s$) as per the standard. Hence, for modulation test, the performance marginally complies with the requirement of P class PMU.

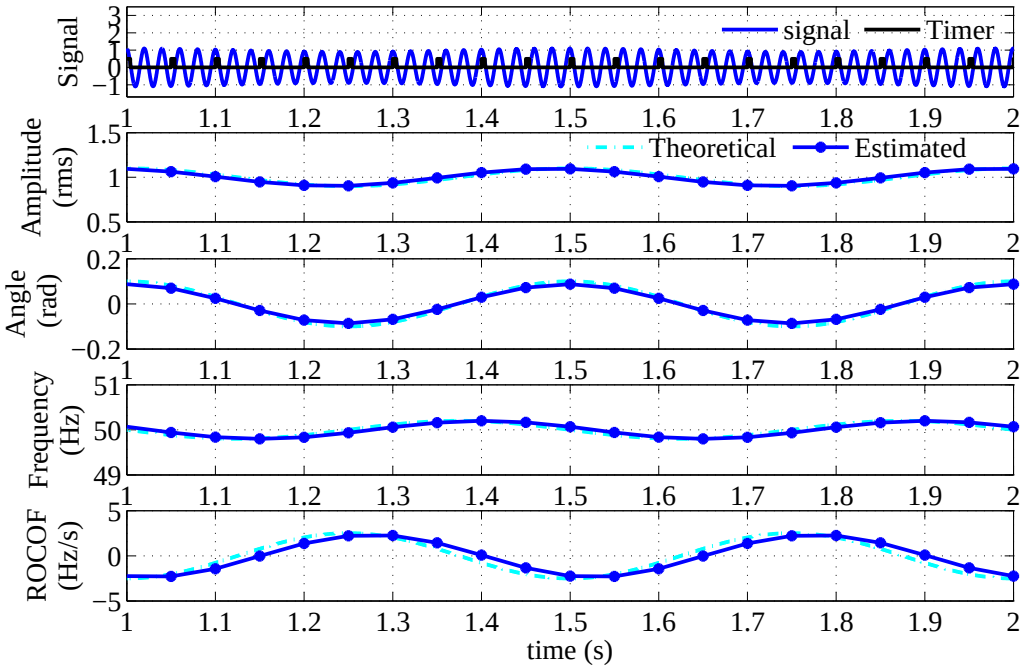

Figure 4.7: Performance of the proposed PMU at sine modulated frequency with $k_x = 0.1$, $k_a = 0.1$ and $f_m = 2Hz$

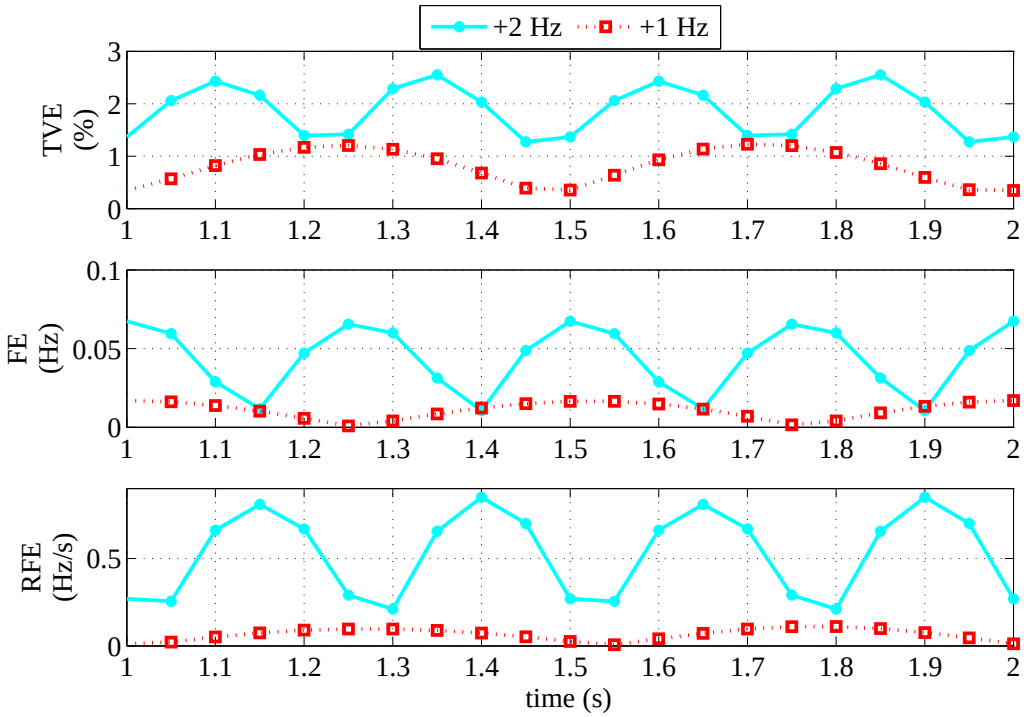

Figure 4.8: Error calculation of the PMU for sine modulated frequency of the input signal with $k_x = 0.1$, $k_a = 0.1$ and $f_m = 2Hz$ and $1Hz$

4.2 Simulation Result of Proposed Method 2

The simulation model of the PMU using this method was developed in MATLAB. The basic features of developed PMU were $N = 24$, $\Delta T = 833.33\mu s$ or sampling frequency($f_s = 1200Hz$), and reporting rate ($F_r = 1200Hz$). The proposed PMU was able to extract the phasor information and frequency of signal for every new sample. The performance of PMU was evaluated for both steady-state and dynamic conditions according to IEEE C37.118.1-2011.

4.2.1 Steady-state Test

The PMU was tested with the input signal of different frequency ranging from 45 to $55Hz$. The measurements were taken at steady-state. The estimation results for off-nominal frequencies above $50Hz$ is shown in Fig. 4.9 and below $50Hz$ is in Fig. 4.10. The accuracy of magnitude and phase angle estimation was checked by TVE which is always less than 1%. This confirmed the compliance with the standard. The frequency and ROCOF estimation was not shown here because, at steady-state they could be determined accurately. These estimations would be shown in dynamic test.

At higher off-nominal frequency, the synchrophasor rotates faster and in both Fig. 4.9 and 4.10, this phenomenon could be observed from angle estimation. Since, the proposed algorithm have separate strategy of interpolation for higher and lower off-nominal frequency, TVE estimated for signal of $45Hz$ and $55Hz$ is not same. Thus, the algorithm is not symmetrical for positive and negative frequency deviations. It can be observed that TVE at $55Hz$ is larger than for $45Hz$, but still under the compliance with the standard.

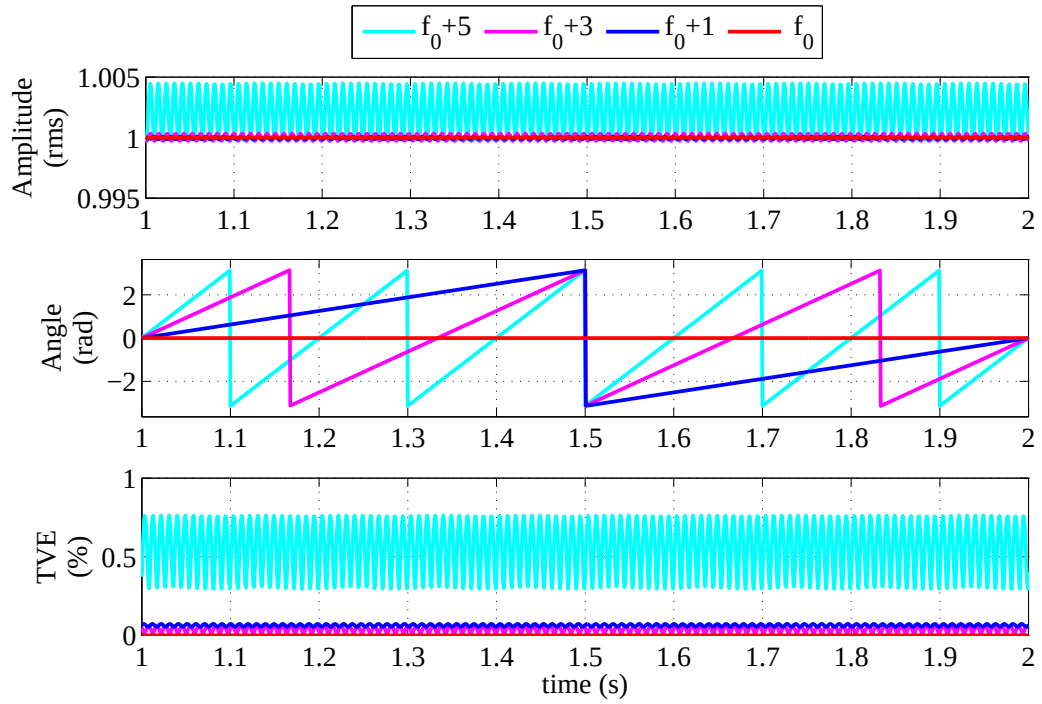

Figure 4.9: Evaluation of the system at various off-nominal frequency above f_0 at steady-state.

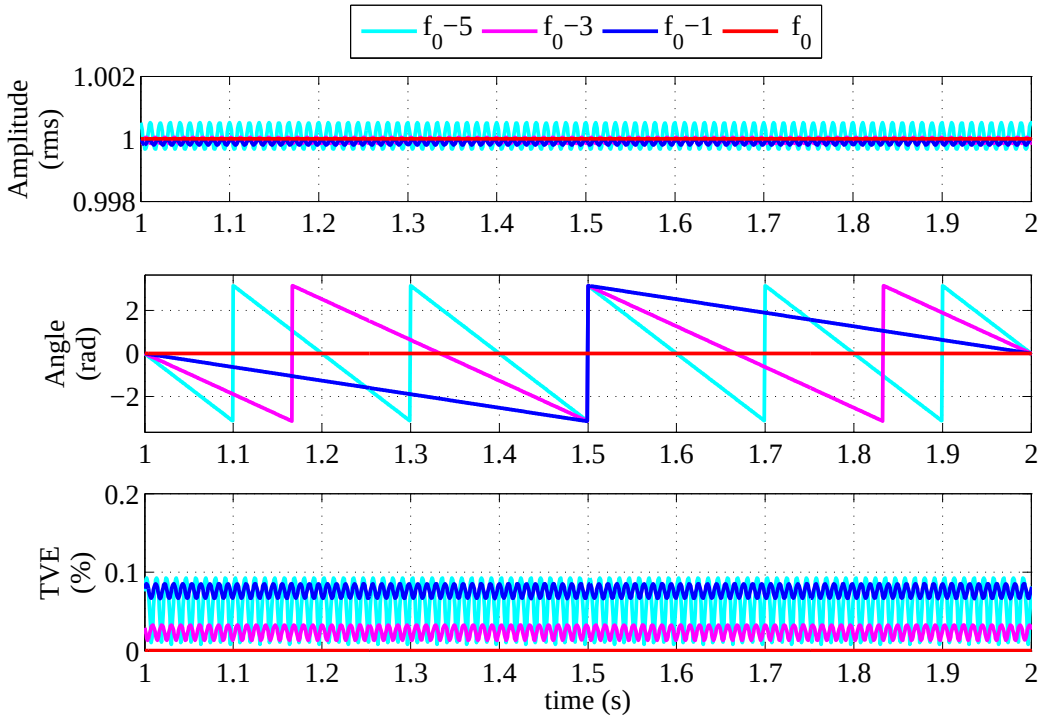

Figure 4.10: Evaluation of the system at various off-nominal frequency below f_0 at steady-state.

4.2.2 Dynamic Test

A. Ramp Frequency Test

The test signal used for this ramp frequency test was as in (4.1). The nominal signal was subjected to frequency ramp of $1Hz/s$ at an instant of $1s$. The estimation result from proposed algorithm was recorded for such input signal. The result of the estimation is presented in Fig. 4.11. The estimated values of amplitude, phase angle, frequency and ROCOF is following the actual values. In ramp condition, the frequency deviation increases with time after the initiation of ramping. Thus the synchrophasor rotation increases in parabolic manner as shown in Fig 4.11, subplot 2. Fig. 4.12, presents the estimation error for different values of ramp rate. The TVE for all ramp rates was found to be less than 1%, which is under the compliance. However, frequency error (FE) was less than $2mHz$, which is higher than that demanded by the standard. The proposed frequency estimator was able to track the system frequency but could not meet the accuracy level of the standard. The rate of change of frequency error (RFE) was less $1Hz/s$ which is in agreement with the standard.

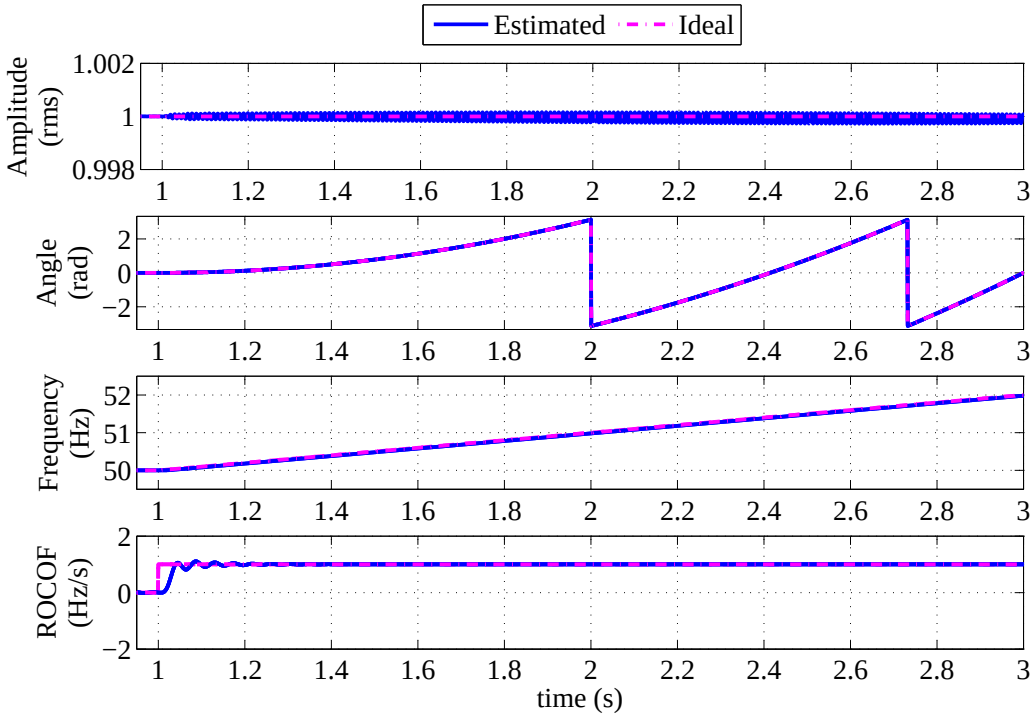

Figure 4.11: Simulation result of ramp frequency of 1 Hz/s initiated at t = 1 second

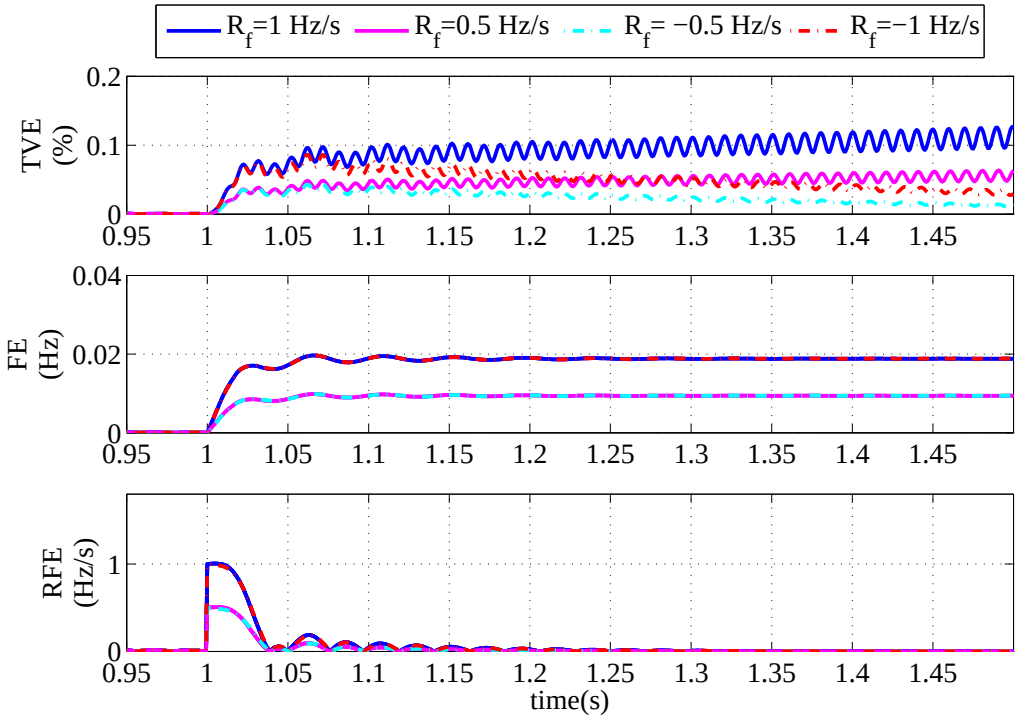

Figure 4.12: Error calculation for the ramp frequency of 1 Hz/s at t = 1 second

B. Modulation Test

The test signal used for this test was as in (4.2). As per the standard, amplitude and phase modulation factor of 0.1 and maximum modulation frequency of $2Hz$ was used in the test signal. The estimation result from the proposed algorithm is illustrated in Fig. 4.13. The proposed algorithm was able to follow the signal amplitude, phase, frequency, and ROCOF despite small lagging was observed in frequency and ROCOF estimation. The errors of estimation is presented in Fig. 4.14, show that the TVE is less than 3%, which is in compliance with the standard. The maximum frequency error for this modulation is $0.05Hz$, which is less than maximum allowed FE ($0.06Hz$) by the standard. Finally, the RFE is less than $1Hz/s$, which is less than maximum allowed RFE ($3Hz/s$) as per the standard. Hence, for modulation test, the performance fully complies with the requirement of P class PMU.

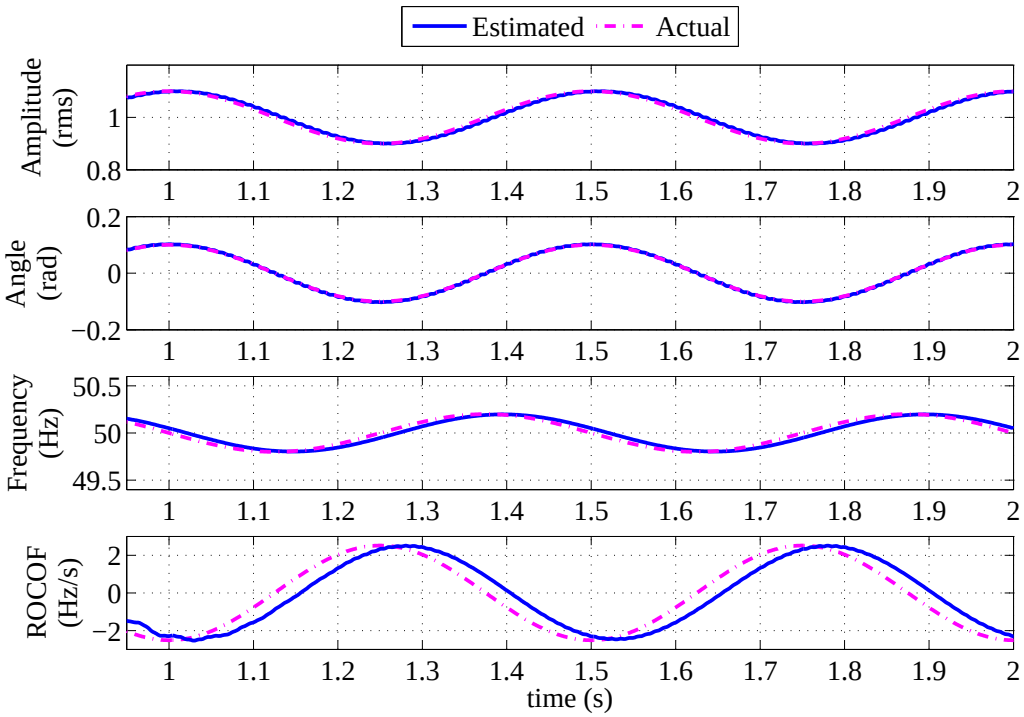

Figure 4.13: Simulation result for amplitude and phase modulated input signal to the the purposed PMU

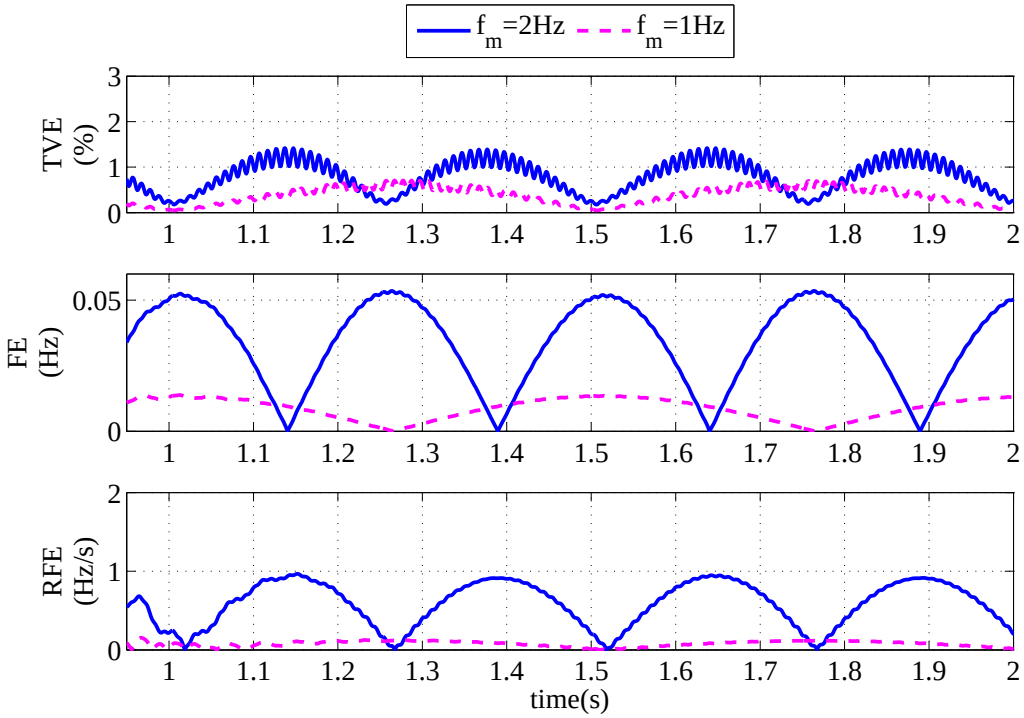

Figure 4.14: Error calculation of the PMU for amplitude and phase modulated input signal

C. Step Test

In power system, the voltage drops or rise due to sudden change of huge loads and due to temporary faults. The sudden changes in amplitude are categorized as electromagnetic transients in power system and induces error in phasor estimator. Such invalid measurements should be identified and avoided. The transient monitoring technique was introduced in [17], to avoid such detect such invalid phasors. However, in this research, we did not deal with filtering the valid and invalid phasors. The purpose of the step test was to ensure the stability of the algorithm.

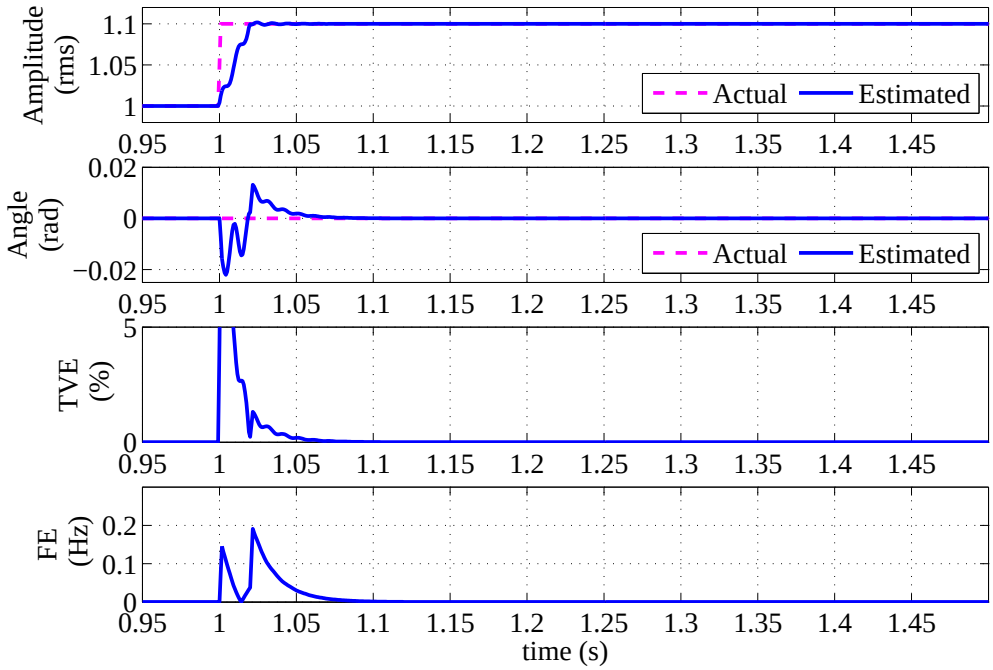

Figure 4.15: Response to amplitude step of 10% at t = 1 second

Due the sudden increment of amplitude, the TVE become very large and it took about 2.5 cycle to give the correct estimation. The step amplitude can be referred as sudden change of one phasor to another. So, the data buffer will contain the data of first phasor and second phasor. This is the main reason of higher TVE during the step transient. It takes at least one cycle to get rid of such mixed data in the buffer [17]. As shown in Fig. 4.15, it took nearly one cycle time and 2.5 cycle time to generate the correct amplitude and angle estimation respectively. Hence, the proposed algorithm is stable for the step test.

4.3 Experimental Setup

The experimental setup mainly consisted of a prototype PMU, signal generator (TG2511), an oscilloscope (DPO 4054B), and LabVIEW 2014 and the schematic is shown in Fig. 4.16. The reference signal was generated from TG2511 using various modes like sweep, trigger and modulation. The extracted phasor along with frequency and ROCOF information from prototype PMU were communicated to the LabVIEW terminal by means of 1 Mbps link setup by RS485 protocol. The labVIEW was used as data visualizer and storage in real time.

The prototype PMU was programmed with the algorithm described in the proposed method 2, which utilized SVA and RLS frequency estimator for PMU design. The advantage of this approach compared to proposed method 1 is that it can generate phasor information for each sampling instant and has higher reporting rate. The higher reporting rate of PMU signifies it ability to measure faster dynamics of the signal. Although proposed method 1 has simple phasor estimation algorithm and performance index is same as proposed method 2, it is not used in experimental setup for this research, mainly due to interest on tracking dynamic condition of the power signal.

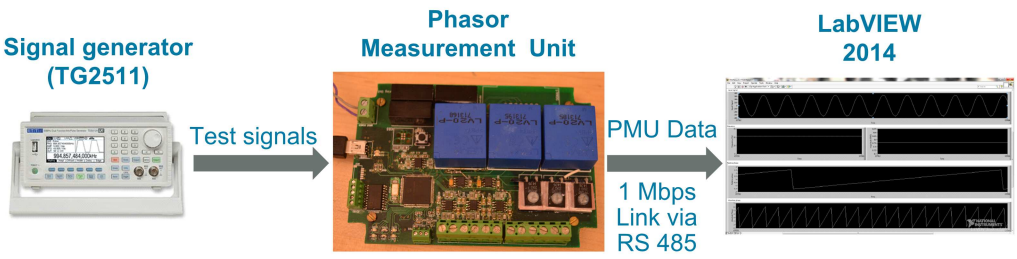

Figure 4.16: Schematic of experimental setup

The prototype PMU had multiple current and voltage sensing ports along with USB and RS485 communication interface. The main heart of the prototype was the digital signal processor (DSP) of microchip family dspic33EP512GM710. It is a multipurpose DSP capable of computing at 70 MIPS. Since the computation was time demanding, Q math was used in place of floating point number. Q math is a approximation of float number, which contributes in the error in estimation too. The PMU data of only 2 digit precision was communicated to the LabVIEW, which would be a major contribution of truncation error. Despite of these approximation and truncation error, TVE for various input signal was evaluated for the recorded PMU data. The prototype PMU was programmed with proposed algorithm with the specification such as $N = 12$, $\Delta T = 1.6666667ms$ or sampling frequency($f_s = 600Hz$), and reporting rate

($F_r = 600Hz$). Due to the limitation of computation speed of the DSP, the sampling frequency of the prototype was reduced by half to that of simulation model.

The National Instruments LabVIEW was used as the data acquisition terminal. The LabVIEW was interfaced with the prototype PMU utilizing the Microchip MCP2200 Configuration utility. The main purpose of this utility was to allow the use RS485 protocol from a USB interface. The LabVIEW processed the received data in real time and visualized the received data in graphical interface. The real-time monitoring of phasor information, along with frequency and ROCOF were the benefits of using LabVIEW.

4.4 Experimental Results

The PMU data from the protoype PMU was received by the LabVIEW and stored. The features such as sampled signal, R.M.S value, frequency, absolute and relative phase of a signal were included in PMU data. The section of recorded data from PMU for the signal of approximately 50 Hz is shown in Fig. 4.17.

s/n	Absolute phase (rad)	R.M.S value (volt)	frequency (Hz)	sampled signal (amplitude quantized value)	Relative phase (rad)
1	4.79	0.78	50.01	26	0.6
2	5.31	0.78	50	195	0.6
3	5.84	0.78	50	310	0.6
4	0.08	0.78	50	343	0.6
5	0.6	0.78	50	283	0.6
6	1.12	0.78	50	145	0.6
7	1.65	0.78	50	-29	0.6
8	2.17	0.78	50	-198	0.6
9	2.69	0.78	50	-312	0.6
10	3.22	0.78	50	-344	0.6
11	3.74	0.78	50.01	-283	0.6
12	4.27	0.78	50.01	-147	0.6
13	4.79	0.78	50.01	27	0.6
14	5.31	0.78	50.01	197	0.6
15	5.84	0.78	50.01	311	0.6
16	0.08	0.78	50.02	342	0.6
17	0.6	0.78	50.02	282	0.6
18	1.13	0.78	50.02	145	0.6
19	1.65	0.78	50.01	-29	0.6
20	2.17	0.78	50.01	-198	0.6

Figure 4.17: Section of the recorded PMU data

Here, absolute phase angle refer to the angle measured with reference to static horizontal line where as relative phase angle is measured with reference to a rotating phasor of nominal frequency (f_0). The sampled signal in the Fig. 4.17 is shown in digitized form.

4.4.1 Result Validation

In order to validate the recorded phasor information, the actual phasor of the signal has to be determined. The true frequency of the signal from the function generator was determined with the Oscilloscope Tektronix DPO 4054B. The oscilloscope was tuned to 20M record length and frequency was determined with good precision. Then the phase angle of the input signal can be determined as:

$$\Phi(n\Delta T) = 2\pi n\Delta T + \phi_0 \tag{4.3}$$

where,

ϕ_0 is an initial phase

The ϕ_0 was used from the experimental data to match the initiation instant for both experimental and theoretical data. Thus, the theoretical phase angle for each sampling time can be computed directly by knowing the precise frequency. The main challenging task was to determine the sampling time precisely. For this, the 8 digit precise sampling time of the PMU was computed with the same oscilloscope and was determined to be $\Delta T = 1.66697966$ millisecond. The total vector error of the estimated phasor was evaluated using (2.1). Fig. 4.18 and 4.19 shows the performance of the protype PMU at various steady state frequencies ranging from 45 to $50Hz$. It was observed that the TVE at nominal frequency was least compared to that for off-nominal frequencies. As the proposed algorithm was unsymmetrical for positive and negative frequency deviation, the TVE for $55Hz$ and $45Hz$ is not same. As seen in the simulation result, the TVE for $55Hz$ is higher than at $45Hz$ for experimental data too. The TVE experimental data was higher than that for simulation due to the approximation error due to Q math and truncation error due to only 2 digit data communication.

Additionally, the ramp test for maximum ramp rate was performed with the same setup. The ramping test was made for a duration until the frequency reaches $55Hz$ and $45Hz$ for $+1Hz/s$ and $-1Hz/s$ respectively. In both positive and negative ramping test shown in Fig. 4.20 and 4.21, the TVE for the entire ramping period is less than 1% as in the simulation results.

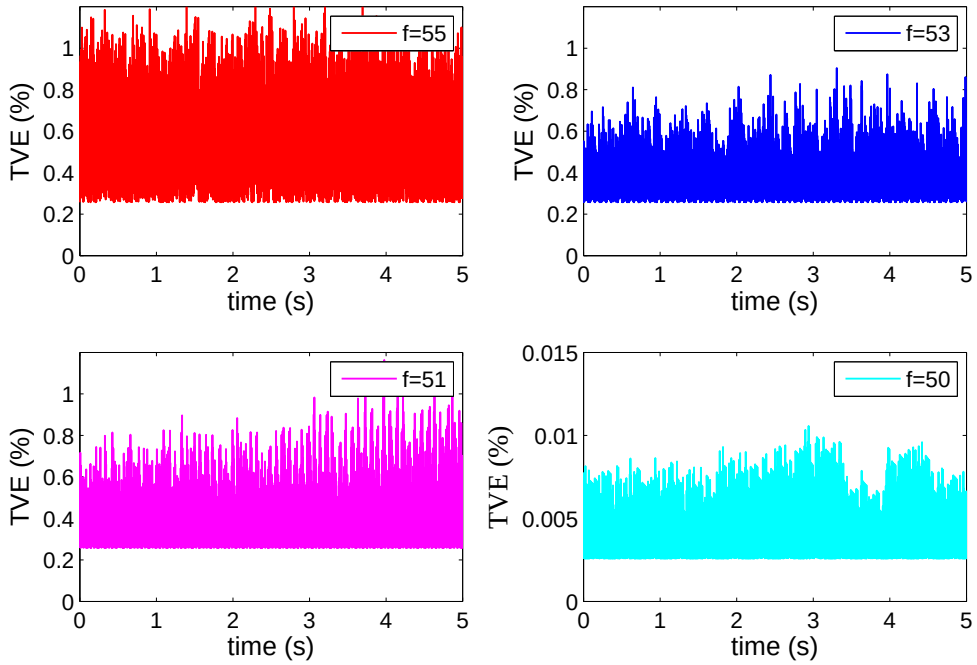

Figure 4.18: Evaluation of TVE of the prototype PMU at higher off-nominal frequencies

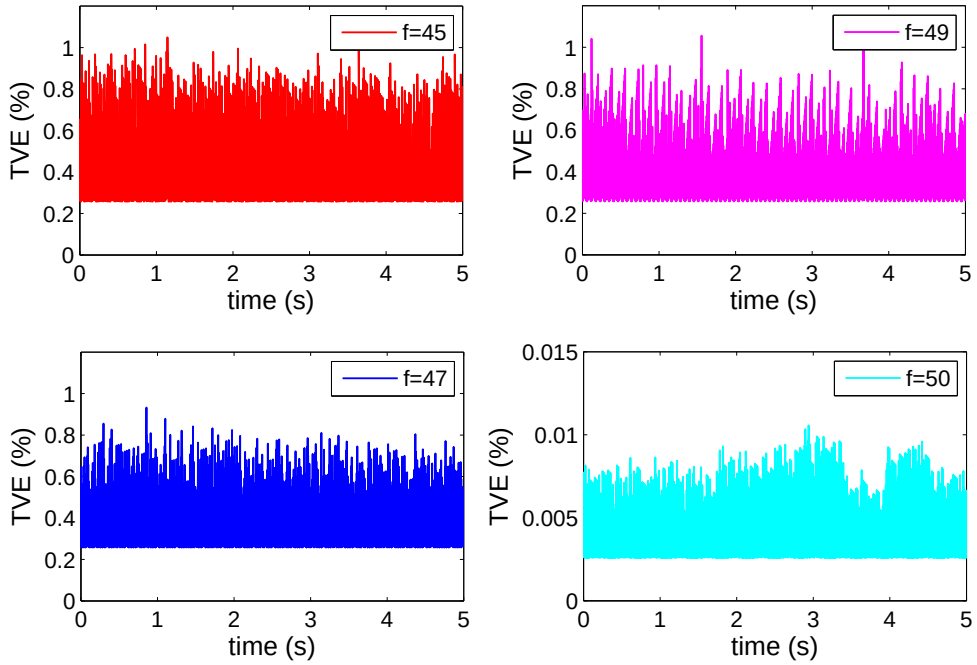

Figure 4.19: Evaluation of TVE of the prototype PMU at lower off-nominal frequencies

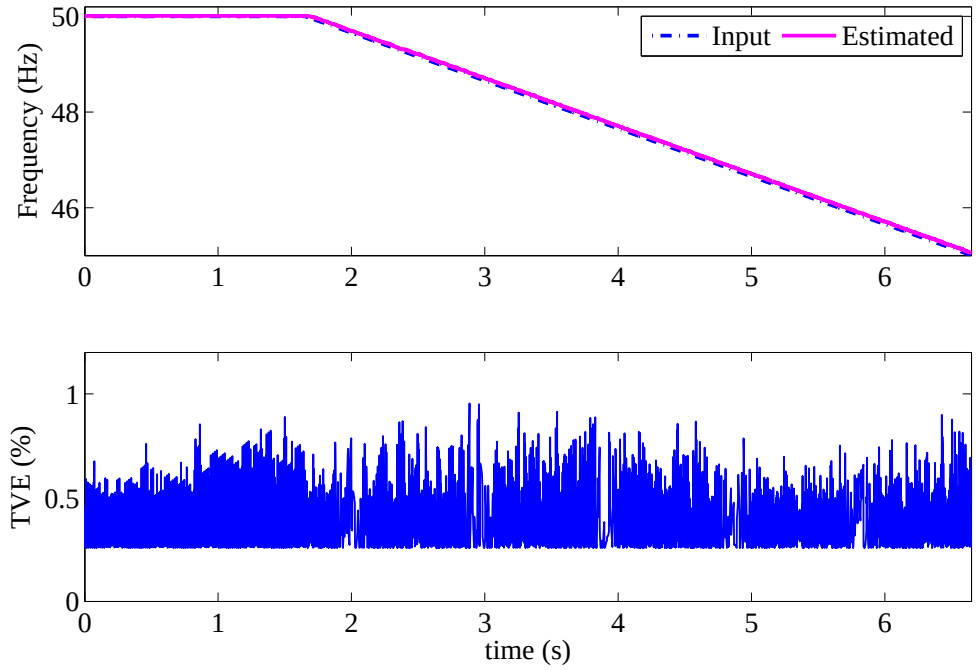

Figure 4.20: Evaluation of TVE of the prototype PMU during frequency ramp of -1 Hz/s

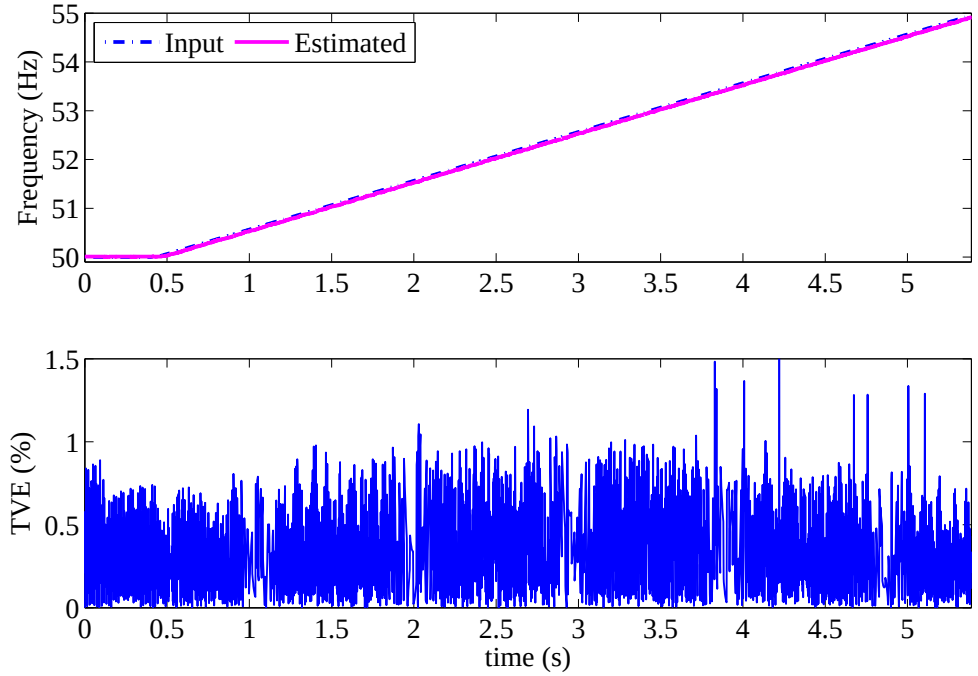

Figure 4.21: Evaluation of TVE of the prototype PMU during frequency ramp of +1 Hz/s

4.5 Discussions

The simulation results of two proposed algorithm for real-time phasor estimation illustrated that the TVE was less than 1% for steady-state and ramping frequency test, where as TVE was less than 3% for modulation test. Thus, TVE comply with both P and M class PMU as per the standard. However, the FE during ramp test could not comply with standard because the frequency estimator employed in both algorithms were averaging estimator. A instantaneous frequency estimator had been used then the algorithm has potential to comply fully with standard. The prototype PMU was implemented using the method 2. The testing was done for nominal and various off-nominal frequencies. The TVE for the measurements were evaluated and shown in Fig. 4.18 and Fig. 4.19. Both the plot shows that TVE increase at higher frequency deviations and is very low at nominal frequency and is less than 1% for frequency deviation of $\pm 5Hz$. Similarly, for the positive and negative ramp of $1Hz/s$, the TVE of the measurement from prototype was found to be less than 1%. The measurement results for phasor computation complied with the standard.

CHAPTER 5

Conclusions and Future Works

5.1 Conclusions

The two algorithms for PMU application were designed by enhancing the conventional DFT with real time window tuning. The first algorithm used sampling time adjustment for tuning which needed a extra internal clock for time synchronization with GPS. The second method used sample value adjustment technique which was based upon the spline approximation. The second method did not need any extra internal clock because the fixed sampling frequency facilitates for synchronizing it with the GPS directly. Frequency information of the signal is a must for window tunning algorithms. For this, the biased Jabcobsen method was implemented in first, where RLS based frequency estimator in second algorithm. The simulation result proved that the TVE was always less than 1% for $\pm 5Hz$ frequency deviation from the nominal value under static conditions. Also, for frequency ramp of $\pm 1Hz/s$ and for standard modulation test, the TVE was still less than 1% and 3%, respectively. The TVE of the proposed method ascertain the algorithm comply with IEEE standard.

The prototype PMU was built with microchip dsPIC33EP512GM710 as the central processor and the LabVIEW was programmed for data acquisition and visualizer. The signal information such as phase angle, frequency and R.M.S value was obtained at real time and offline validation was conducted. The TVE of the prototype PMU for the frequency range of $45Hz$ to $55Hz$ at steady state was under 1%. Similarly, the ramp frequency was also tested with

the same PMU and the TVE was less than 1% for both ± 1 Hz/s ramp rate. Hence, the proposed phasor computing algorithm were able to extract the phasor information at both steady and dynamic state with the performance index complying to the IEEE C37.118.1-2011.

5.2 Future Works

The main limitation of the proposed PMU was with frequency estimator because the dynamic phasor computation requires instantaneous frequency. Most of the proposed frequency estimator works on principle of FFT or RLS method, which are averaging techniques. This incurs delay in frequency estimation which is significant during the system dynamics. Although, most literature neglects this delay assuming the power system dynamics are slower, the synchrophasor standard for PMU demands higher accuracy even for faster dynamics. The estimation accuracy could be significantly improved with instantaneous frequency estimation.

In the prototype design, we used low end signal processor from microchip which cost only several dollars. The demerit of such DSP is that the precision of ADC is not more than 10 bits and do not have enhanced floating point support. Due to which we had to utilize the Q math. Q math is approximation of a floating number and contributes approximation error in measurement, but the advantage is computational efficiency. The another source of error was limiting the precision of transmitted measurements with 2 digit. This has to be done considering the time demanding calculation of the PMU algorithm and the calculation speed of the DSP. The truncated data transmission were also the source of error in phasor evaluation form the PMU. The experiment TVE could have been far lower than 1% with higher precision of data transmission. Hence, for complying fully with P and M class PMU, the instantaneous frequency estimation has to be implemented and DSP should be upgraded.

APPENDIX A

Abbreviations

PMU Phasor Measurement Unit

GPS Global Positioning System

UTC Universal Coordinated Time

TVE Total Vector Error

ROCOF Rate of Change of Frequency

RFE Rate of Change of Frequency Error

FE Frequency Error

CRLB CramerRao lower bound

FFT Fast Frequency Transformation

MLE Maximum Likelihood Estimator

RLS Recursive Least Squares

FDR Frequency Disturbance Recorder

DFT Discrete Fourier Transformation

SVA Sample Value Adjustment

PPS Pulse per Second

Bibliography

[1] B. Liscouski and W. Elliot, ”Final report on the august 14, 2003 blackout in the united states and canada: Causes and recommendations,” A report to US Department of Energy, vol. 40, 2004.

[2] E. C. R. Council, ”The economic impacts of the August 2003 blackout,” Washington, DC, 2004.

[3] G. Andersson, P. Donalek, R. Farmer, N. Hatziargyriou, I. Kamwa, P. Kundur, et al., ”Causes of the 2003 major grid blackouts in North America and Europe, and recommended means to improve system dynamic performance,” IEEE Transactions on Power Systems, vol. 20, pp. 1922-1928, 2005.

[4] J. G. Kassakian, R. Schmalensee, G. Desgroseilliers, T. D. Heidel, K. Afridi, A. Farid, et al., ”The future of the electric grid,” Massachusetts Institute of Technology, Tech. Rep, 2011.

[5] S. Eftekharnejad, V. Vittal, G. T. Heydt, B. Keel, and J. Loehr, ”Impact of increased penetration of photovoltaic generation on power systems,” IEEE Transactions on Power Systems, vol. 28, pp. 893-901, 2013.

[6] D. Gautam, V. Vittal, and T. Harbour, ”Impact of increased penetration of DFIG-based wind turbine generators on transient and small signal stability of power systems,” IEEE Transactions on Power Systems, vol. 24, pp. 1426-1434, 2009.

[7] G. Rogers, Power system oscillations: Springer Science & Business Media, 2012.

[8] B. Wojszczyk, ”Deployment of advanced Smart Grid solutions - Global examples & lessons learned,” in Innovative Smart Grid Technologies (ISGT), 2012 IEEE PES, 2012, pp. 1-1.

[9] J. Bertsch, M. Zima, A. Suranyi, C. Carnal, and C. Rehtanz, ”Experiences with and perspectives of the system for wide area monitoring of power systems,” in Quality and Security of Electric Power Delivery Systems, 2003. CIGRE/PES 2003. CIGRE/IEEE PES International Symposium, 2003, pp. 5-9.

[10] D. Novosel and K. Vu, ”Benefits of PMU technology for various applications,” Zbornik radova sedmog simpozija o sustavu vodenja EES-a HK CIGRE, Cavtat, vol. 5, 2006.

[11] I. A. Hiskens, ”Nonlinear dynamic model evaluation from disturbance measurements,” IEEE Transactions on Power Systems, vol. 16, pp. 702-710, 2001.

[12] L. Chun-Hao and N. Ansari, ”The Progressive Smart Grid System from Both Power and Communications Aspects,” Communications Surveys & Tutorials, IEEE, vol. 14, pp. 799-821, 2012.

[13] L. Dosiek, J. W. Pierre, and J. Follum, ”A Recursive Maximum Likelihood Estimator for the Online Estimation of Electromechanical Modes With Error Bounds,” IEEE Transactions on Power Systems, vol. 28, pp. 441-451, 2013.

[14] N. K. C. Nair, J. C. H. Peng, and R. Sherry, ”Synchrophasors and supporting infrastructure in New Zealand transmission grid,” in Power and Energy Society General Meeting, 2011 IEEE, 2011, pp. 1-5.

[15] G. Missout and P. Girard, ”Measurement of bus voltage angle between Montreal and Sept-Iles,” IEEE Transactions on Power Apparatus and Systems, pp. 536-539, 1980.

[16] P. Bonanomi, ”Phase angle measurements with synchronized clocks-principle and applications,” IEEE Transactions on Power Apparatus and Systems, pp. 5036-5043, 1981.

[17] A. G. Phadke and J. S. Thorp, Synchronized phasor measurements and their applications: Springer Science & Business Media, 2008.

[18] M. Model, ”1690 PMU Disturbance Recorder,” Clifton Park, NY, Macrodyne.

[19] ”IEEE Standard for Synchrophasors for Power Systems,” IEEE Std C37.118-2005 (Revision of IEEE Std 1344-1995), pp. 1-57, 2006.

[20] ”IEEE Standard for Synchrophasor Measurements for Power Systems,” IEEE Std C37.118.1-2011 (Revision of IEEE Std C37.118-2005), pp. 1-61, 2011.

[21] A. G. Phadke and J. S. Thorp, Computer relaying for power systems: John Wiley & Sons, 2009.

[22] E. Brigham and R. Morrow, ”The fast Fourier transform,” Spectrum, IEEE, vol. 4, pp. 63-70, 1967.

[23] Y. Xu and B. Ju, ”Synchronized phasor measuring method using recursive DFT with a window function,” in Transmission and Distribution Conference and Exhibition: Asia and Pacific, 2005 IEEE/PES, 2005, pp. 1-6.

[24] A. Borghetti, C. A. Nucci, M. Paolone, G. Ciappi, and A. Solari, ”Synchronized phasors monitoring during the islanding maneuver of an active distribution network,” IEEE Transactions on Smart Grid, vol. 2, pp. 82-91, 2011.

[25] D. Macii, D. Petri, and A. Zorat, ”Accuracy analysis and enhancement of DFT-based synchrophasor estimators in off-nominal conditions,” IEEE Transactions on Instrumentation and Measurement, vol. 61, pp. 2653-2664, 2012.

[26] A. Phadke and B. Kasztenny, ”Synchronized phasor and frequency measurement under transient conditions,” IEEE Transactions on Power Delivery, vol. 24, pp. 89-95, 2009.

[27] P. M. Anderson and A. A. Fouad, Power system control and stability: John Wiley & Sons, 2008.

[28] M. Akke and J. S. Thorp, ”Sample value adjustment improves phasor estimation at off-nominal frequencies,” IEEE Transactions on Power Delivery, vol. 25, pp. 2255-2263, 2010.

[29] D. Hart, D. Novosel, Y. Hu, B. Smith, and M. Egolf, ”A new frequency tracking and phasor estimation algorithm for generator protection,” IEEE Transactions on Power Delivery, vol. 12, pp. 1064-1073, 1997.

[30] G. Benmouyal, ”An adaptive sampling-interval generator for digital relaying,” IEEE Transactions on Power Delivery, vol. 4, pp. 1602-1609, 1989.

[31] G. C. Zweigle, L. S. Anderson, and A. Guzman-Casillas, ”Apparatus and method for estimating synchronized phasors at predetermined times referenced to an absolute time standard in an electrical system,” ed: Google Patents, 2009.

[32] A. Guzman-Casillas and G. C. Zweigle, ”Protective relay with synchronized phasor measurement capability for use in electric power systems,” ed: Google Patents, 2005.

[33] J. Xi and J. F. Chicharo, ”A new algorithm for improving the accuracy of periodic signal analysis,” IEEE Transactions on Instrumentation and Measurement, vol. 45, pp. 827-831, 1996.

[34] M. Karimi-Ghartemani, B.-T. Ooi, and A. Bakhshai, ”Application of enhanced phase-locked loop system to the computation of synchrophasors,” IEEE Transactions on Power Delivery, vol. 26, pp. 22-32, 2011.

[35] M. A. Platas-Garza and J. A. de la O Serna, ”Dynamic harmonic analysis through Taylor Fourier transform,” IEEE Transactions on Instrumentation and Measurement, vol. 60, pp. 804-813, 2011.

[36] J. Ren and M. Kezunovic, ”Real-time power system frequency and phasors estimation using recursive wavelet transform,” IEEE Transactions on Power Delivery, vol. 26, pp. 1392-1402, 2011.

[37] S. Haykin, Communication systems: John Wiley & Sons, 2008.

[38] P. H. Dana and B. M. Penrod, ”The role of GPS in precise time and frequency dissemination,” GPS World, vol. 1, 1990.

[39] H. L. Van Trees, Detection, estimation, and modulation theory: John Wiley & Sons, 2004.

[40] M. D. Macleod, ”Fast nearly ML estimation of the parameters of real or complex single tones or resolved multiple tones,” IEEE Transactions on Signal Processing, vol. 46, pp. 141-148, 1998.

[41] B. G. Quinn, ”Estimating frequency by interpolation using Fourier coefficients,” IEEE Transactions on Signal Processing, vol. 42, pp. 1264-1268, 1994.

[42] B. G. Quinn, ”Estimation of frequency, amplitude, and phase from the DFT of a time series,” IEEE Transactions on Signal Processing, vol. 45, pp. 814-817, 1997.

[43] S. Provencher, ”Estimation of complex single-tone parameters in the DFT domain,” IEEE Transactions on Signal Processing, vol. 58, pp. 3879-3883, 2010.

[44] E. Jacobsen and P. Kootsookos, ”Fast, accurate frequency estimators,” IEEE Signal Process. Mag, vol. 24, pp. 123-125, 2007.

[45] C. Candan, ”A method for fine resolution frequency estimation from three DFT samples,” Signal Processing Letters, IEEE, vol. 18, pp. 351-354, 2011.

[46] Y. Liao, ”Phase and Frequency Estimation: High-Accuracy and Low-Complexity Techniques,” Worcester Polytechnic Institute, 2011.

[47] M. M. Begovic, P. M. Djuric, S. Dunlap, and A. G. Phadke, ”Frequency tracking in power networks in the presence of harmonics,” IEEE Transactions on Power Delivery, vol. 8, pp. 480-486, 1993.

[48] A. Abdollahi and F. Matinfar, ”Frequency estimation: a least-squares new approach,” IEEE Transactions on Power Delivery, vol. 26, pp. 790-798, 2011.

[49] A. Lopez, J.-C. Montano, M. Castilla, J. Guti?rrez, M. D. Borras, and J. C. Bravo, ”Power system frequency measurement under nonstationary situations,” IEEE Transactions on Power Delivery, vol. 23, pp. 562-567, 2008.

[50] Q. W. Jia, ”Disturbance rejection through disturbance observer with adaptive frequency estimation,” IEEE Transactions on Magnetics, vol. 45, pp. 2675-2678, 2009.

[51] C. S. Turner, ”Slope filtering: An FIR approach to linear regression [DSP Tips&Tricks],” Signal Processing Magazine, IEEE, vol. 25, pp. 159-163, 2008.